Development and Demonstration of a 25 Watt Thermophotovoltaic Power Source for a Hybrid Power System

Edward Doyle, Kailash Shukla, and Christopher Metcalfe
Thermo Power Corporation, Waltham, Massachusetts

Since its founding, NASA has been dedicated to the advancement of aeronautics and space science. The NASA Scientific and Technical Information (STI) Program Office plays a key part in helping NASA maintain this important role.

The NASA STI Program Office is operated by Langley Research Center, the Lead Center for NASA's scientific and technical information. The NASA STI Program Office provides access to the NASA STI Database, the largest collection of aeronautical and space science STI in the world. The Program Office is also NASA's institutional mechanism for disseminating the results of its research and development activities. These results are published by NASA in the NASA STI Report Series, which includes the following report types:

- TECHNICAL PUBLICATION. Reports of completed research or a major significant phase of research that present the results of NASA programs and include extensive data or theoretical analysis. Includes compilations of significant scientific and technical data and information deemed to be of continuing reference value. NASA's counterpart of peer-reviewed formal professional papers but has less stringent limitations on manuscript length and extent of graphic presentations.

- TECHNICAL MEMORANDUM. Scientific and technical findings that are preliminary or of specialized interest, e.g., quick release reports, working papers, and bibliographies that contain minimal annotation. Does not contain extensive analysis.

- CONTRACTOR REPORT. Scientific and technical findings by NASA-sponsored contractors and grantees.

- CONFERENCE PUBLICATION. Collected papers from scientific and technical conferences, symposia, seminars, or other meetings sponsored or cosponsored by NASA.

- SPECIAL PUBLICATION. Scientific, technical, or historical information from NASA programs, projects, and missions, often concerned with subjects having substantial public interest.

- TECHNICAL TRANSLATION. English-language translations of foreign scientific and technical material pertinent to NASA's mission.

Specialized services that complement the STI Program Office's diverse offerings include creating custom thesauri, building customized data bases, organizing and publishing research results . . . even providing videos.

For more information about the NASA STI Program Office, see the following:

- Access the NASA STI Program Home Page at *http://www.sti.nasa.gov*

- E-mail your question via the Internet to help@sti.nasa.gov

- Fax your question to the NASA Access Help Desk at 301–621–0134

- Telephone the NASA Access Help Desk at 301–621–0390

- Write to:
  NASA Access Help Desk
  NASA Center for AeroSpace Information
  7121 Standard Drive
  Hanover, MD 21076

Development and Demonstration of a 25 Watt Thermophotovoltaic Power Source for a Hybrid Power System

Edward Doyle, Kailash Shukla, and Christopher Metcalfe
Thermo Power Corporation, Waltham, Massachusetts

National Aeronautics and
Space Administration

Glenn Research Center

Available from

NASA Center for Aerospace Information
7121 Standard Drive
Hanover, MD 21076

National Technical Information Service
5285 Port Royal Road
Springfield, VA 22100

Available electronically at http://gltrs.grc.nasa.gov/GLTRS

Table of Contents

List of Figures

List of Tables

Development and Demonstration of a 25 Watt Thermophotovoltaic Power Source for a Hybrid Power System

Edward Doyle, Kailash Shukla, and Christopher Metcalfe
Thermo Power Corporation
Waltham, Massachusetts 02454

The development of a propane-fueled, 25 W thermophotovoltaic (TPV) power source for use in a hybrid power system is described. The TPV power source uses a platinum emitting surface with an anti-reflective coating to radiate to gallium antimonide photocells, which converts the radiation to electric power. The development program started with the design and fabrication of an engineering prototype system. This was used as a component development vehicle to develop the technologies for the various components. A 25 W demonstration prototype was then designed and fabricated using the most advanced component approaches. The designs and test results from this development program are discussed.

1.0 EXECUTIVE SUMMARY

The objective of the program was to develop a propane-fueled, 25 W thermophotovoltaic (TPV) power source for use in a hybrid power system. The hybrid power system would combine the TPV power source with a military BB-390 A/U rechargeable battery to produce a maximum power capability of 111 W with a 25 W recharge rate.

The TPV power source uses a platinum emitting surface with an anti-reflective coating to radiate to gallium antimonide (GaSb) photocells, which converts the radiation to electric power. The system efficiency is improved by the use of dielectric filters on the GaSb cells for optical energy recovery and a recuperator for thermal energy recovery.

The development program started with the design and fabrication of an engineering prototype system. This was used as a component development vehicle to develop the technologies for the various components. A 25 W demonstration prototype was then designed and fabricated using the most advanced component approaches. The designs and test results from this development program are discussed in this report.

The components for the demonstration prototype and the assembled demonstration prototype are shown below. It produced a maximum power of 28 W. The demonstration prototype had an overall gross efficiency of 3.0%. With further development, it would be possible to raise this efficiency to 6-7% principally by using more advanced dielectric filters, reducing heat losses from the system and using a smaller, higher temperature emitter.

2.0 INTRODUCTION

Thermophotovoltaic (TPV) energy conversion, which uses PV cells to directly convert radiant thermal energy into electric power, has a number of important advantages for portable power generation in both military and commercial applications. Since TPV is a direct energy conversion technology with no moving parts in the energy conversion system, it has the potential to provide quiet, reliable, maintenance-free electric power for thousands of hours. It also has the potential to be efficient, operate on military logistic fuels, and start and operate in sub-freezing environments.

At a TPV workshop conducted for the Army Research Office in July 1996, several potential applications of TPV for the Army were identified. One of these was as a substitute for batteries such as the BA-5590. This primary (non-rechargeable) battery and its rechargeable alternatives are useable in many military platforms, and represent a significant fraction of the cost for the batteries purchased by the Army.

The performance characteristics of the BA-5590 primary battery and one of its rechargeable alternatives, the BB-390A/U, are presented in Table 1. While these batteries are identical in size and configuration, the weight of the rechargeable BB-390A/U battery is 65% higher than the primary BA-5590 battery. The capacity of the rechargeable BB-390A/U is also only 47% of the BA-5590 primary battery.

TABLE 1. Battery Performance Specifications

Specifications	BA-5590 Battery	BB-390 A/U Battery
Dimensions (l×w×h), in	4.4×2.45×5.0	Same
Volume, in^3	53.9	Same
Weight, lb	2.33	3.85
Max. Current, amps	4/2	7.2/3.6
Nominal Voltage, volts	12/24	Same
Max. Power, watts	48	86
Storage Capacity, w-h	163	77

The Army purchases large quantities of these batteries to meet its needs for both military missions and for training. For military missions, the lower weight and higher stored energy of the BA-5590 primary battery makes it the preferred choice. For training, rechargeable batteries are being used more often because they can be recharged hundreds of times thereby making their life-cycle costs much lower. The higher weight and lower stored energy of rechargeable batteries requires more batteries and a higher weight for the soldier to train for the same mission. The time to recharge the batteries is also an issue.

The overall goal of the program described in this report is to develop a propane-fueled TPV power source suitable for replacement of the BA-5590 primary battery and rechargeable batteries such as the BB-390 A/U. The TPV battery substitute system is expected to have significant advantages, when compared to electrochemical batteries. It will result in a lower weight and volume system for most military missions, will be instantaneously rechargeable, and will have environmental benefits when it comes to disposal.

3.0 DESCRIPTION OF TPV HYBRID POWER SYSTEM

The TPV battery substitute system is comprised of a 25-watt TPV power source used in combination with a BB-390A/U rechargeable battery to make a hybrid power system. It will use replaceable propane fuel cartridges to provide an immediate recharging capability. This combination of a TPV power source with a rechargeable battery has the capability to provide both high instantaneous power and high stored energy and to substitute for BA-5590 and BB-390A/U batteries in many military missions and for military training. When fully developed, the hybrid power system will be capable of providing 111 watts maximum power with a 25-watt recharge rate. The three main elements of this hybrid power system (25-watt TPV power source, BB-390 A/U rechargeable battery, and fuel supply) are illustrated in Figure 1.

25W TPV
POWER SOURCE

BB-390 A/U
RECHARGEABLE
BATTERY
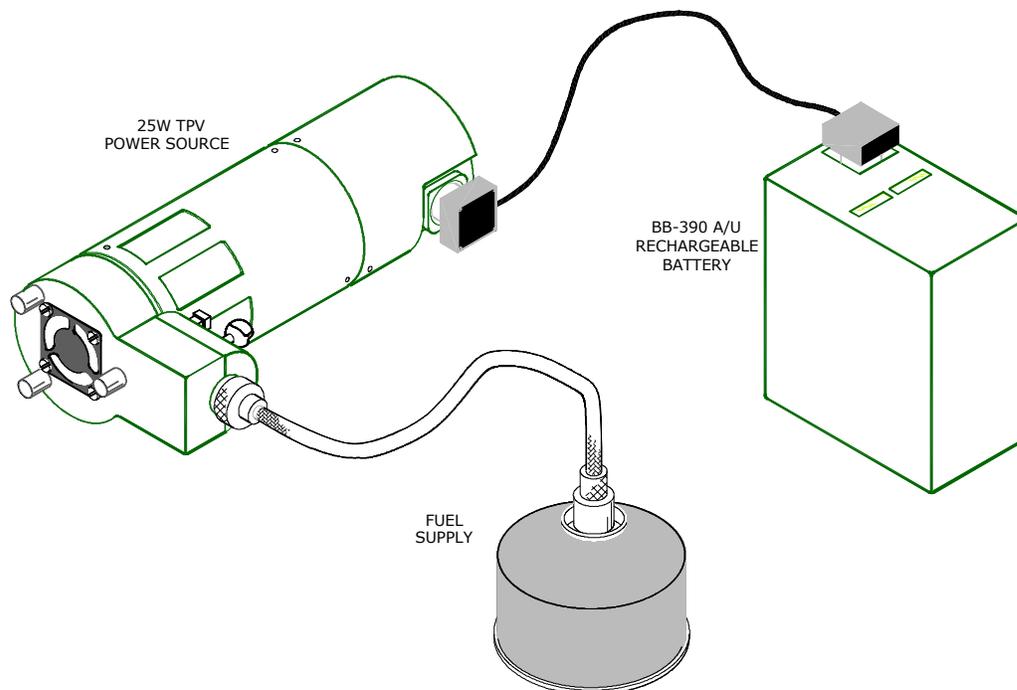
FUEL
SUPPLY

Figure 1. 25 W TPV Hybrid Power System

The electric stored energy capacity (wh) of the TPV hybrid power system is time dependent since the stored energy for the TPV power source is in the form of fuel energy and must be converted to electric energy by the TPV power source. The time dependent capacity of the TPV hybrid power system is presented in Figure 2 based on using a 20-watt TPV power source with a 7% net system efficiency.
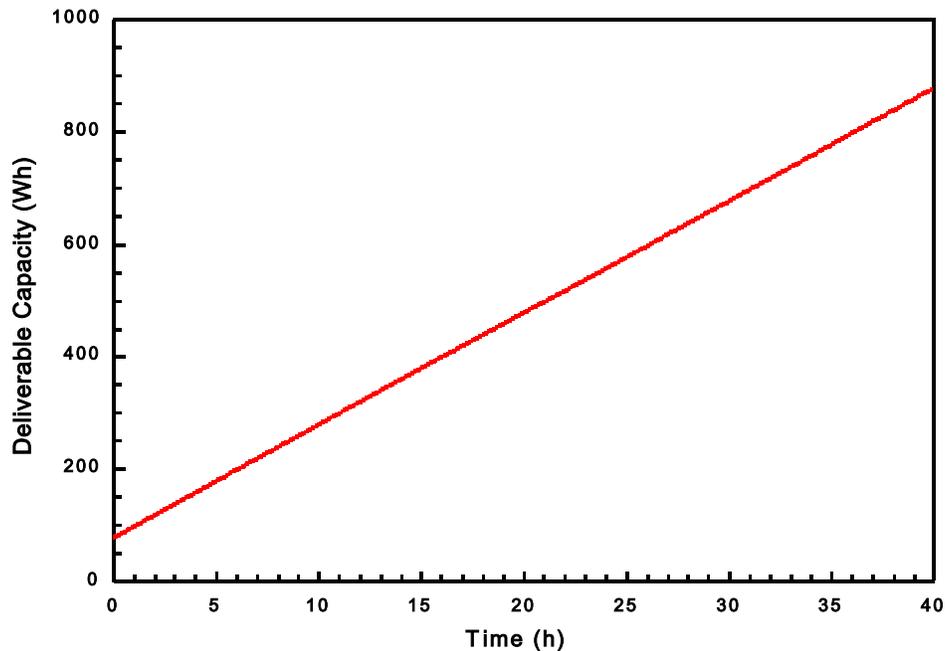
Figure 2. TPV Hybrid Power System Capacity for 20 W TPV Power Source

3.1 Power Source Design

3.1.1 Design Constraints
In designing the TPV power source, the following constraints were placed on the design:

- **Environmental**
  - can be exposed to and submerged under water
  - combustion and cooling air may have contaminants that can damage the emitter, optical filter, and PV cells
- **Orientation**
  - must be capable of operation in any orientation

The approach taken to meet these design constraints is to use a hermetically sealed power conversion module. With this approach, the emitting surface, optical filter and PV cells are contained within a hermetically sealed enclosure to prevent exposure to water and ambient air. This approach excludes the use of flow-through emitters where combustion gases directly contact the emitting surface. This design approach is also suitable for future conversion to liquid fuels that may have contaminants potentially damaging to components.

The key features of the TPV power source design are:

- ***Hermetically Sealed Power Conversion Module***
  - allows enclosed space to be evacuated or charged with inert gas, thereby reducing thermal convection losses
  - provides close packaging for high view factor
  - permits use of tungsten, which would oxidize in air, as the wavelength-selective (for gallium antimonide cells) emitting surface

- ***Fuel Pressure Powered Combustion System***
  - Fuel pressure used in a jet pump to inspirate combustion air, thereby eliminating the need for a combustion blower

- ***Orientation Independence***
  - Forced convection cooling of the PV array and a fuel pressure powered combustion system allow the system to be orientation independent

The design specifications for the TPV power source are presented in Table 2.

Table 2. Design Specifications

PV Cell Type	GaSb
Emitter Type	Selective
Emitter Temperature	1700 K
In-band PV Cell Efficiency	30%
Off-band Optical Recovery	75%
Thermal Recuperator Effectiveness	70%
Air Preheat Temperature	1350 K
Power Output	20 W, Net
System Efficiency	7%, Net

3.2 Power Conversion Module Design Configurations Investigated

The power conversion module, which is comprised of the burner-emitter-recuperator (BER) assembly, PV array, and air-cooled heat sink is illustrated schematically in Figure 3. The direction of flow of the combustion air and exhaust gas is shown on the figure. The way in which the module is hermetically sealed is also illustrated. The hermetically sealed module has two basic subassemblies; the heat sink with the array, and the BER. These two subassemblies are joined together by a flanged connection and sealed with a metallic o-ring for the initial prototypes. Ultimately this would be a welded seal.
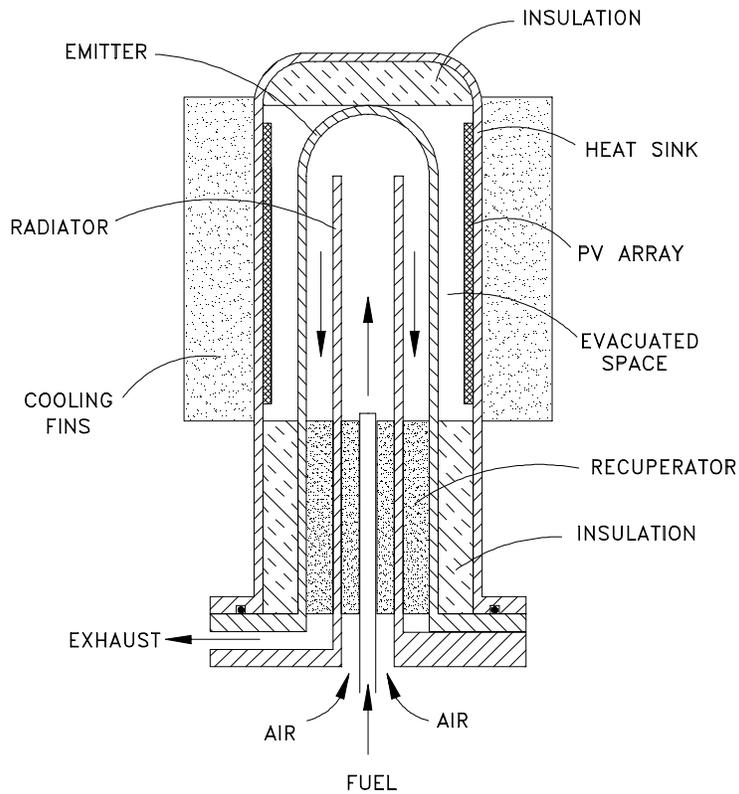
Figure 3. Power Conversion Module Schematic

Two package configurations were studied for the TPV power source during the design phase of the program. These were a rectangular package and a cylindrical package. Except for the cooling fins on the heat sink, the components used in each package configuration were identical for the study.

A schematic for the rectangular package is shown in Figure 4. With this configuration, cross-flow fins are used on the heat sink. This allows the cooling fan and motor to be located to the side of the power conversion module with the fuel controls and piezoelectric igniter located below the fan and motor. This is the more compact packaging approach. This approach, however, has more difficult cooling air flow distribution problems to solve, through the use of air baffles, and could result in greater non-uniformity with respect to the temperature of individual PV cells.

Figure 5 shows the schematic for the cylindrical package. Axial-flow fins are used on the heat sink with this configuration. This allows the cooling fan and motor to be located directly above and on the same axis as the power conversion module. The fuel controls and igniter are located below the power conversion module. This approach produces a somewhat less compact package, but results in very uniform cooling air flow distribution and greater uniformity with respect to the temperature of individual PV cells.
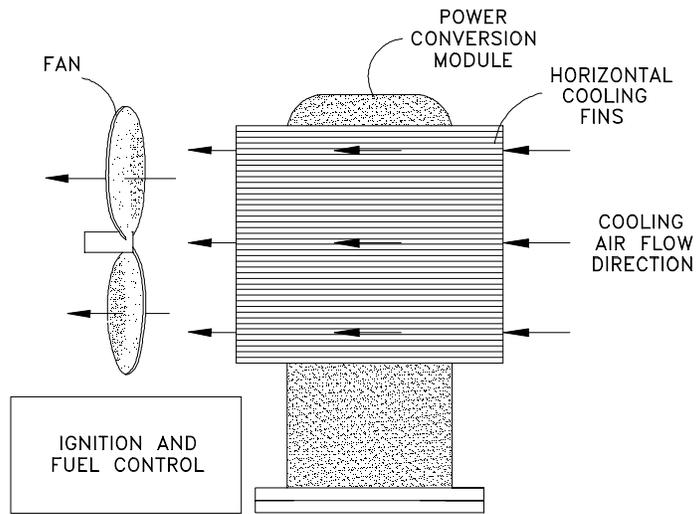
Figure 4. Rectangular Package Schematic
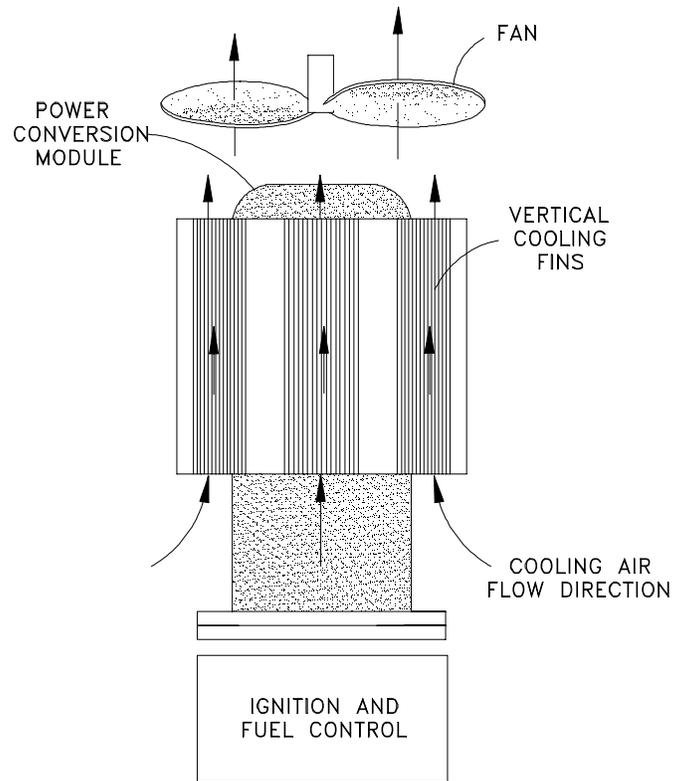
Figure 5. Cylindrical Package Schematic

An exploded view of the rectangular package design is shown in Figure 6, and an exploded view of the cylindrical package design is shown in Figure 7. The various components of the TPV power source are labeled on each of the drawing.
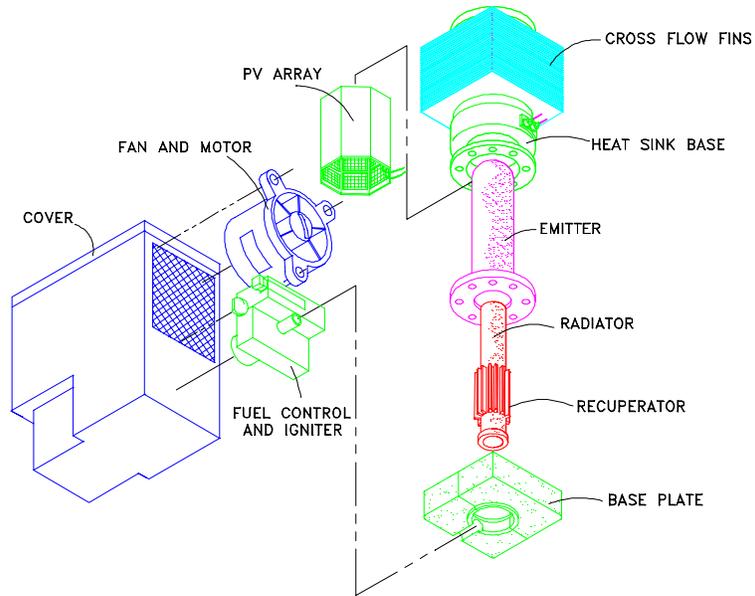
Figure 6. Rectangular Package Design
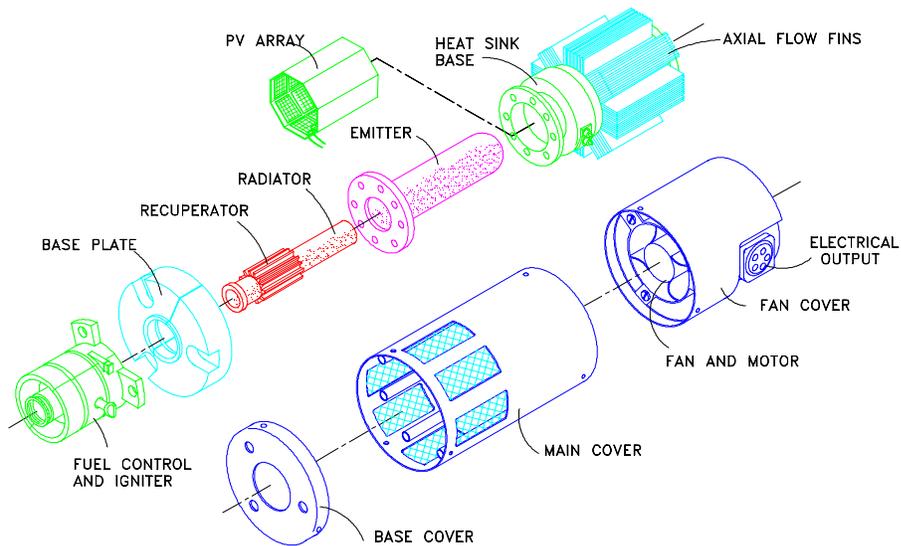
Figure 7 - Cylindrical Package Design

The cylindrical package design approach was selected for the development of the TPV power source because it provided greater flexibility in the design of components and more uniform cooling of the heat sink, which is very important for the overall performance of the system.

3.3 Projected Performance Characteristics

The projected performance characteristics for the TPV hybrid power system, with respect to weight and volume, are presented in Figures 8 and 9. Figure 8 shows the system weight as a function of capacity for the TPV hybrid power system (including fuel and fuel cartridge), for BA-5590 primary batteries, and for BB-390A/U rechargeable batteries. The numbers of each type of battery needed to obtain a given capacity are shown on the figure. For military training or military missions using rechargeable BB-390A/U batteries, the TPV battery substitute system provides a lower weight system if more than one rechargeable battery is required. For military missions using BA-5590 primary batteries, the TPV hybrid power system provides a lower weight system if more than three primary batteries are needed to perform the mission. Figure 9 shows the system volume as a function of capacity for the TPV hybrid power system (including fuel and fuel cartridge), for BA-5590 primary batteries, and for BB-390A/U rechargeable batteries. The conclusions with respect to system volume are similar with the TPV hybrid power system having a lower volume when more than two rechargeable batteries or three primary batteries are needed for the mission.
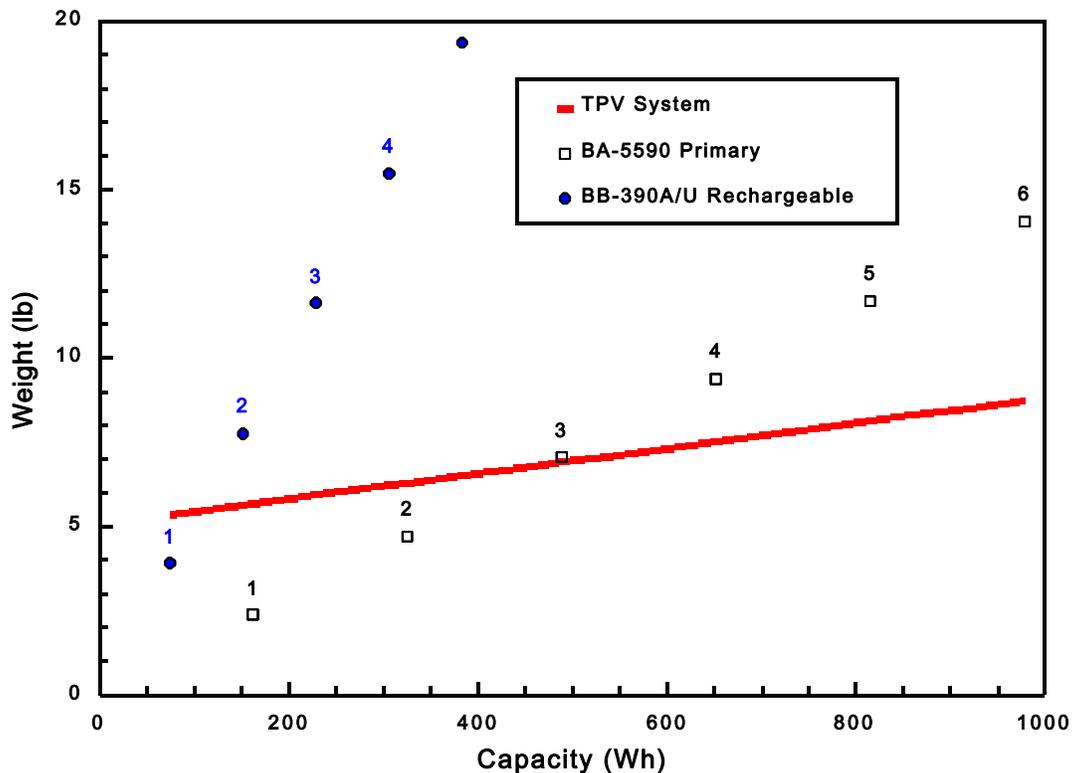
Figure 8. Weight Comparison
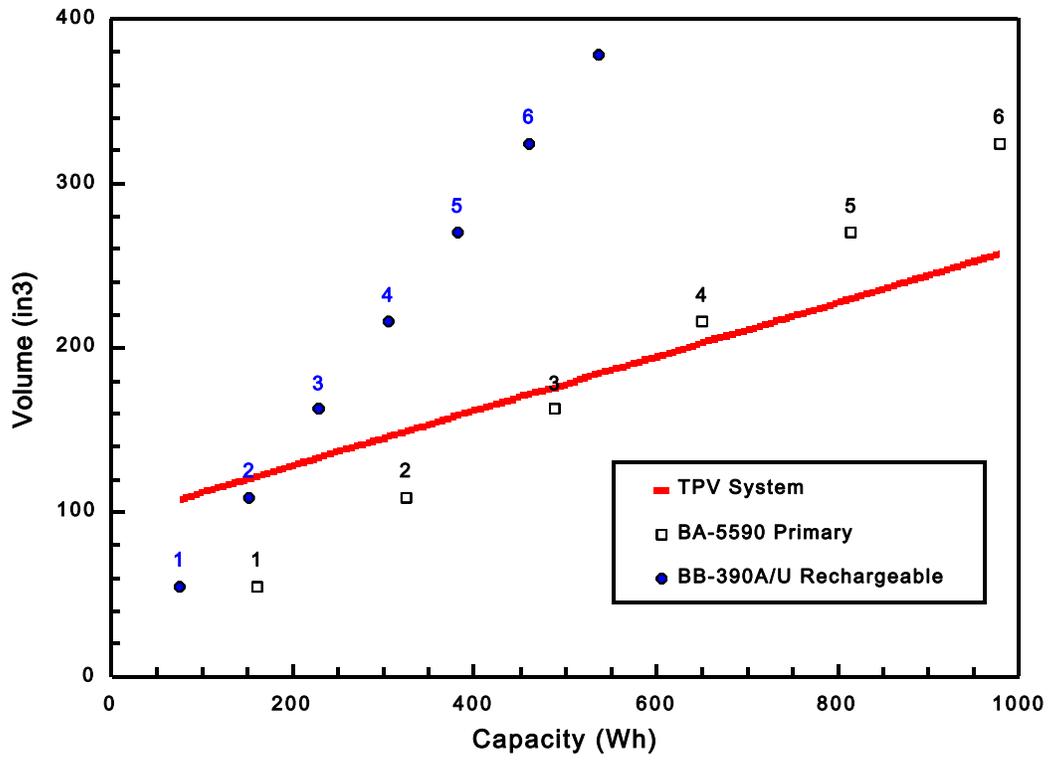
Figure 9. Volume Comparison

4.0 DEVELOPMENT APPROACH

This program undertook the development of only the TPV power source for the hybrid power system. The approach taken was to develop the technology in the laboratory with an <u>engineering prototype</u> TPV power source and to demonstrate the technology with a <u>demonstration prototype</u> TPV power source, which incorporated the most advanced features.

The basic design of the two prototypes is quite similar and differs mainly in individual component details. The TPV power source is cylindrical is design and is approximately three inches in diameter by twelve inches long. An exploded view of the engineering prototype was shown previously in Figure 7. The design layout of the demonstration prototype is shown in Figure 10. Table 3 identifies the main components of each system and the key features and differences in these components for both the engineering prototype and demonstration prototype.
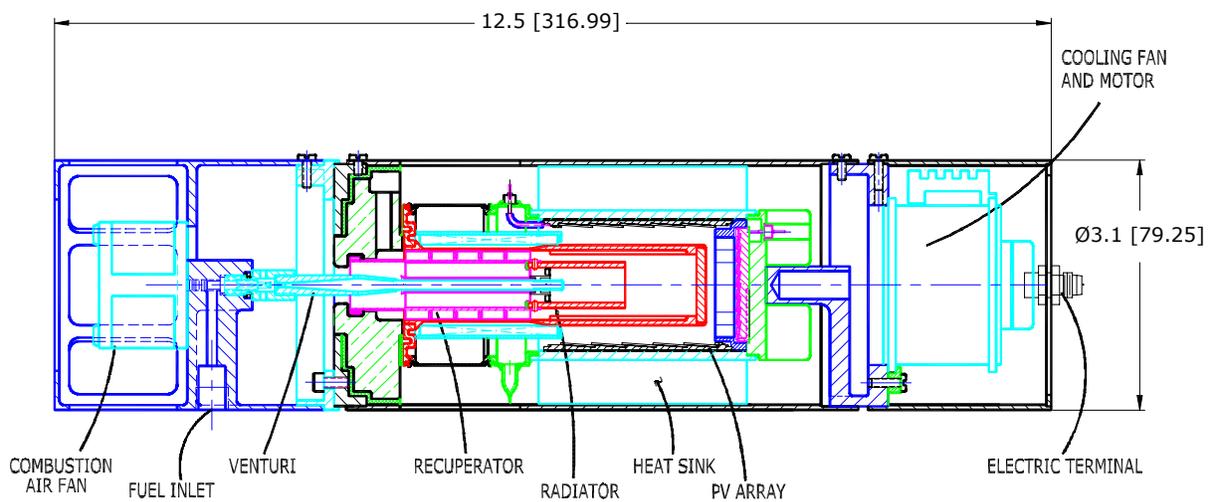
Figure 10. Layout of Demonstration Prototype

The engineering prototype development and the demonstration prototype development will be discussed separately in the next two chapters.

Table 3 - Prototype Comparison Table

Component	Engineering Prototype	Demonstration Prototype
Emitter/PV Array Cavity	Vacuum-tight Air or Argon Charged	Designed for Hermetic Sealing with Inert Gas Charge Operated Vented to Air
PV Array	40 Cell Octagonal Cylinder Flat Circuits - 75% Packing Factor Active Area - 42.3 cm^2 Gold Reflectors Over Inactive Area	40 Cell Octagonal Cylinder and 44 Cell Flat Circular End Disk Shingled Circuits - 100% Packing Factor Active Area - 64.3 cm^2 (52% Increase)
Filters	Dielectric Filter on Cover Glass	Dielectric Filters Integral with Cells
Emitters	Kanthal Tungsten Surface on Silicon Carbide AR Coated Tungsten on Kanthal AR-Platinum Foil Re-radiator Around Kanthal Base Emitter	AR-Coated Platinum Foil Re-radiator Around Kanthal Base Emitter
Recuperator	Inconel Axial Segmented Finned Tube	Inconel Axial Segmented Finned Tube with 25% Increase in Length and Heat Transfer Area
Heat Sink	Air Cooled with Fan Axial Convoluted Copper Fin Stock Joined to Copper Base with Epoxy	Air Cooled with Fan Axial Copper Fins Integral with Copper Base
Combustion System	High Air Preheat, Single-ended Tube with Internal Radiator 20% Primary Air Delivered Mixed with Propane 80% Separately Delivered Through Recuperator	High Air Preheat, Single-ended Tube with Internal Radiator 15% Primary Air Delivered Mixed with Propane 85% Separately Delivered Through Recuperator
Fuel and Air Delivery	Laboratory Supply	Propane Powered Venturi Delivers Primary Air Fan Delivers Secondary Air

5.0 ENGINEERING PROTOTYPE DEVELOPEMENT

A picture of the assembled engineering prototype is shown in Figure 11. A laboratory fuel and air supply is used to operate this prototype. The cover over the fan has been removed to show the fan. The cooling air from the fan flows over the heat sink fins and mixes with the exhaust before exiting from the slots on the left. The edges of the heat sink fins are visible through the slots.
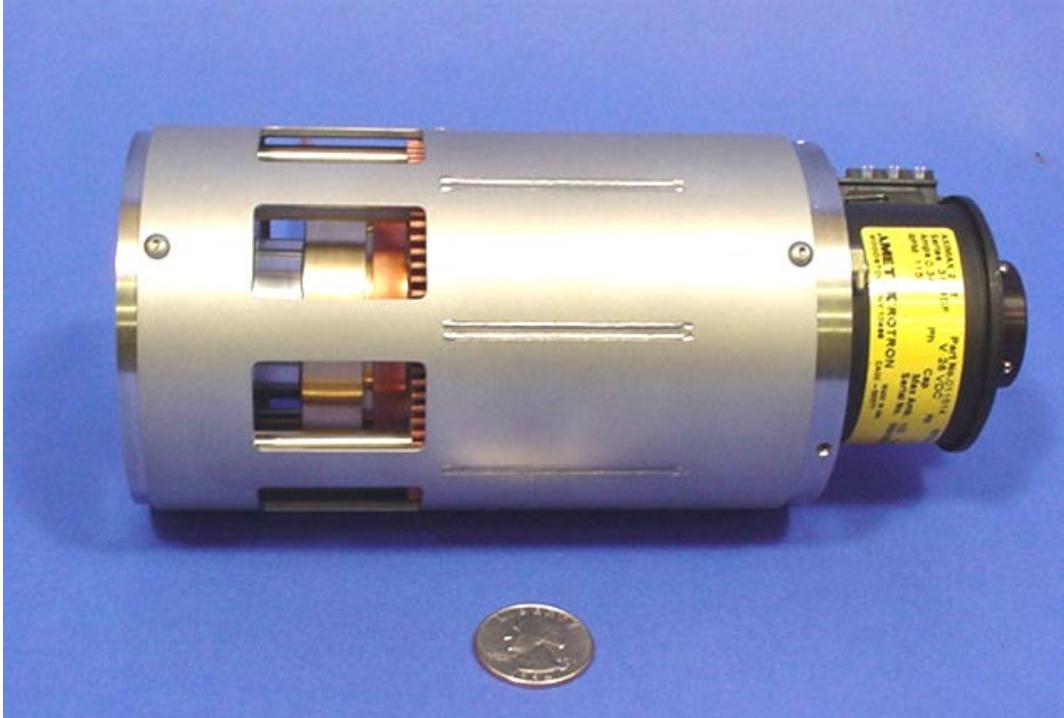
Figure 11 – Engineering Prototype

The eight (8) individual circuits, which make up the PV array for the engineering prototype, are shown in Figure 12. Each circuit has five (5) gallium antimonide cells wired in series. The cells and electrical interconnections have a cover glass over them and are not visible in the picture. The cover glass has the dielectric optical filter deposited directly on it over the cells. There is a gold reflector on one edge of the cover glass, which covers the ~ 25% inactive area where the electrical interconnections are made.

The PV array and heat sink assembly for the engineering prototype, with the eight- (8) circuits installed, is shown in Figure 13. The top cover and bottom housing for the PV array are also shown. These parts are gold plated on the inside to reflect stray radiation back to the emitter.

JX Crystals conducted flash tests on the circuits prior to installing them in the heat sink. The flash test results for one set of eight (8) circuits are given in Table 4. The eight (8) circuits were quite uniform in performance with an average open-circuit voltage (Voc) of 2.45 V, short-circuit current (Isc) of 2.51 A, and fill factor (FF) of 0.69. The flash test results and the current – voltage (I-V) curve for the complete PV array are presented in Figure 14. The measured Isc and FF are only slightly less than the average for the individual circuits and the Voc only slightly less than eight times the average for the individual circuits.
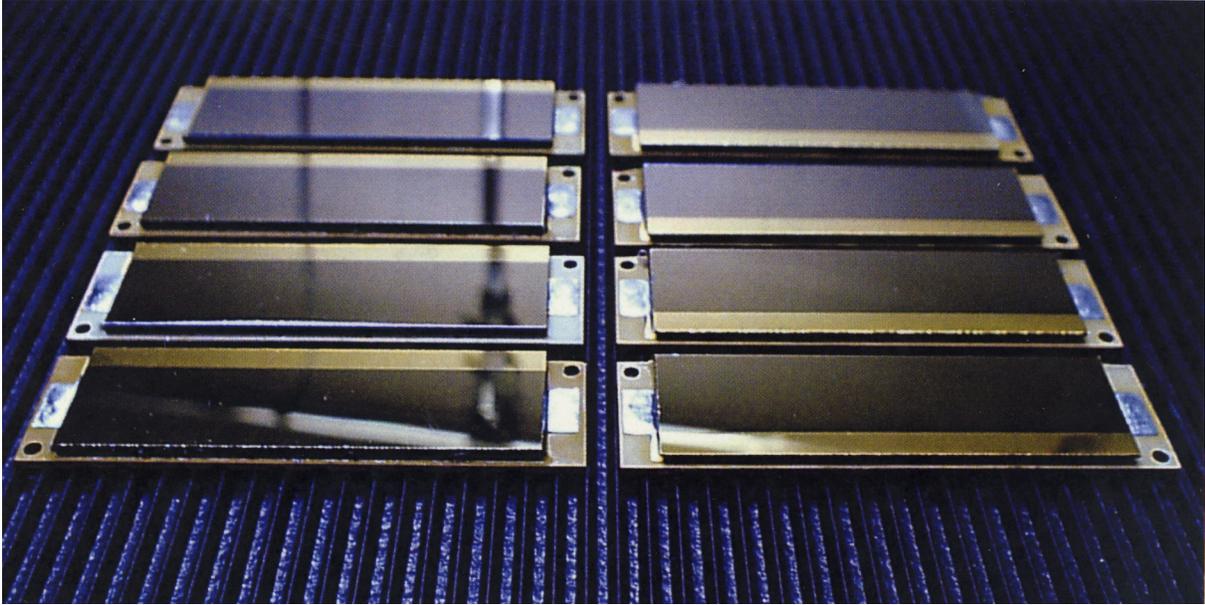
Figure 12 – PV Array Circuits for Engineering Prototype
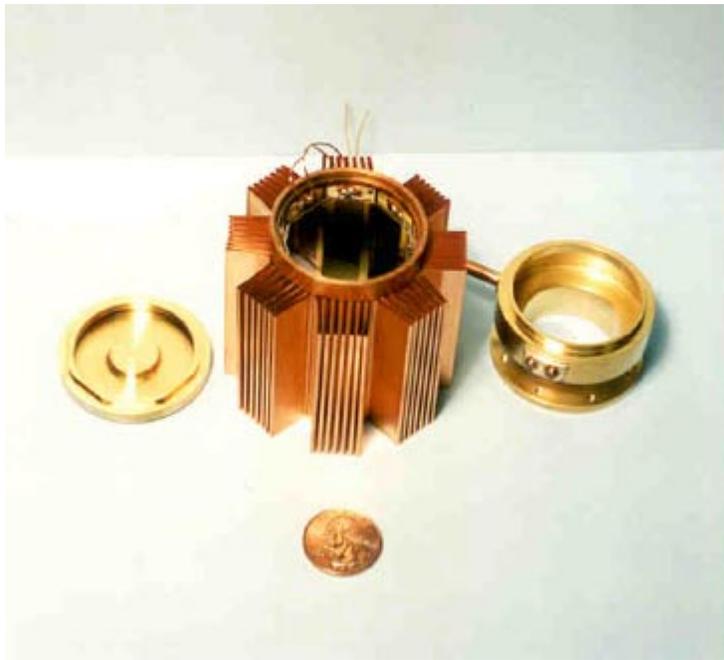
Figure 13 – PV Array and Heat Sink Assembly for Engineering Prototype

Table 4 – Engineering Prototype PV Array Circuit Flash Test Performance

ID	FF	Voc	Isc	Imax	Vmax	Pmax
23	0.69	2.46	2.46	2.11	1.97	4.16
24	0.70	2.45	2.42	2.09	1.97	4.12
25	0.69	2.44	2.30	2.05	1.89	3.89
26	0.70	2.46	2.65	2.35	1.92	4.52
27	0.70	2.42	2.44	2.16	1.90	4.10
28	0.69	2.46	2.59	2.29	1.92	4.39
29	0.70	2.46	2.68	2.39	1.93	4.60
30	0.70	2.44	2.52	2.24	1.92	4.30
Avg	0.69	2.45	2.51	2.21	1.93	4.26

FF	0.66	
Voc	19.17	volts
Isc	2.46	amps
Imax	2.05	amps
Vmax	15.19	volts
Pmax	31.15	watts
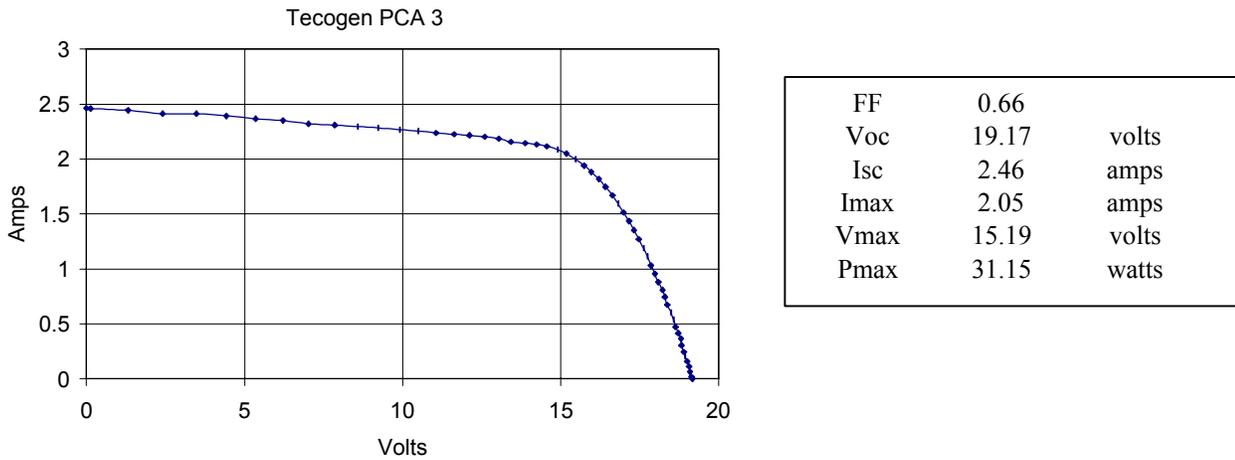
Figure 14 – PV Array Characteristics for Engineering Prototype

The transmissivity for the dielectric filter is presented in Figure 15. The transmissivity in the in-band range from 1.0-1.7 microns is over 90% and drops rapidly an average of less than 10% from 2.0-3.0 microns. It then rises to an average of about 60% beyond 4.0 microns. This substantially reduces the heat load on the PV cells and reflects a significant portion of this radiation back to the emitter.
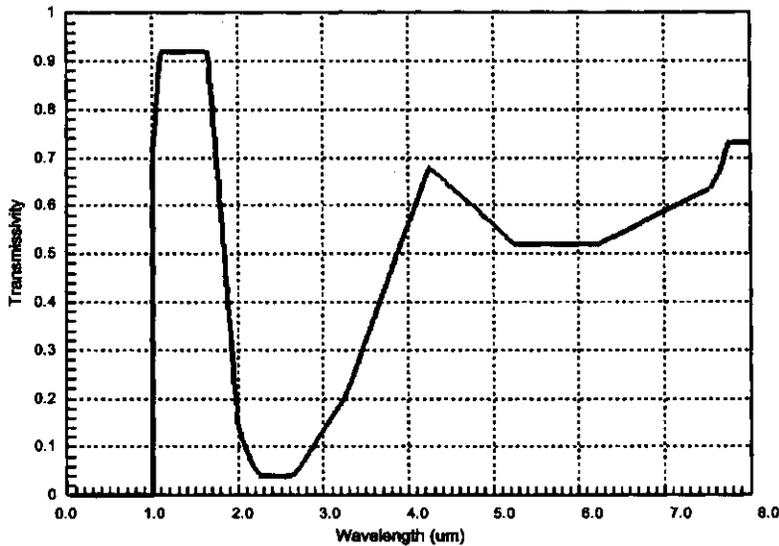
Figure 15 – Transmissivity of Dielectric Filter for Engineering Prototype

The heat sink for the engineering prototype was designed using the computational fluid dynamics (CFD) model "FLUENT". Pressure drop and heat transfer measurements were then made on the heat sink using a laboratory air supply and compared to the model results. The cold pressure drop as a function of airflow results is compared in Figure 16 and shows good agreement with the predictions. The temperatures rise (heat sink mounting surface – average air temperature) as a function of heat load is compared in Figure 17. At the design heat load of 200 W, the actual
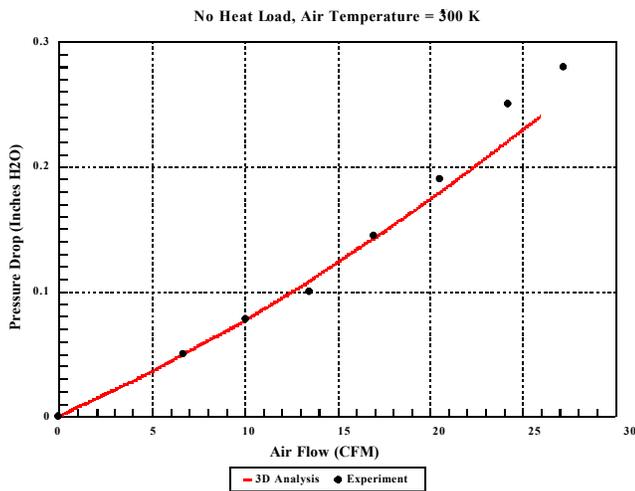
Figure 16 Heat Sink Pressure Drop
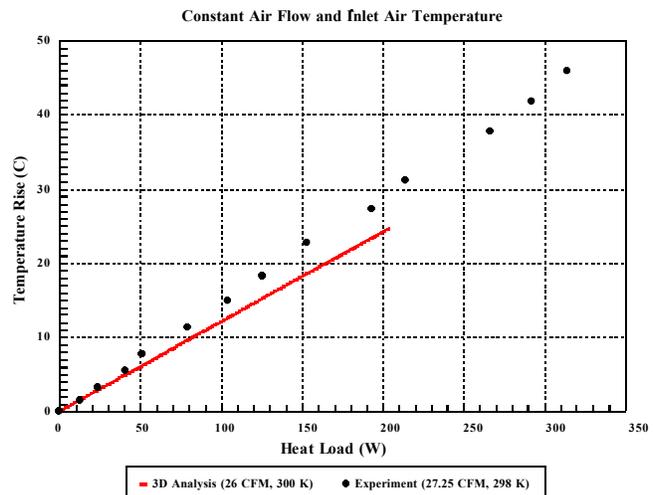
Figure 17 Heat Sink Temperature Rise

temperature rise is 30°C compared to the design value of 25°C, but still well within the acceptable range. The hot pressure drop is shown in Figure 18 as a function of heat load for constant airflow and inlet air temperature. The hot pressure drop is significantly higher than predicted at the design airflow of 26 CFM. The hot pressure drop can be readily reduced back to the design level by lowering the airflow without any significant increase in the temperature rise as shown on Figure 19.
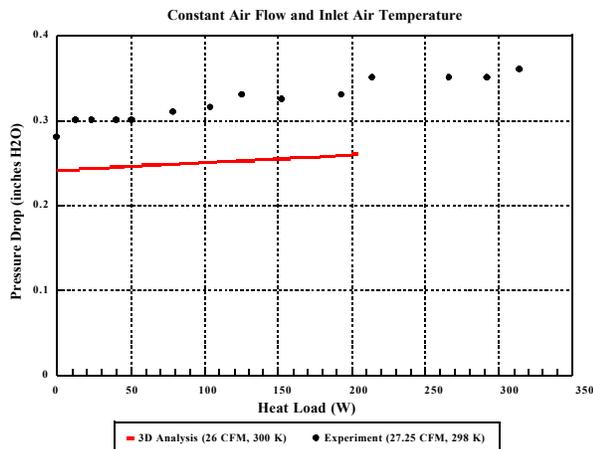
Figure 18 Heat Sink Pressure Drop vs Heat Load
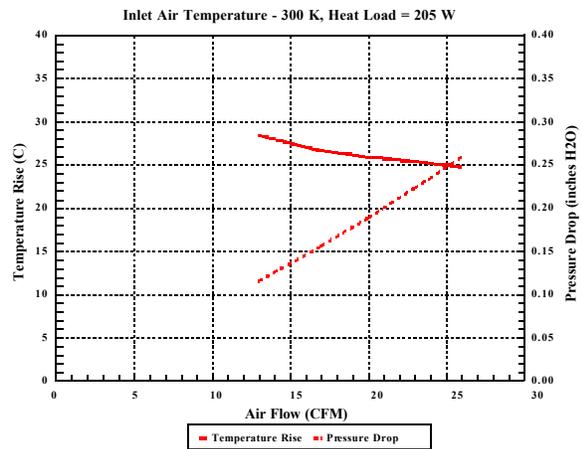
Figure 19 Temperature & Pressure vs Air Flow

The fan that supplies cooling air to the heat sink is shown on Figure 20. It operates at 9,800 rpm at 24 VDC and requires 0.276 A. This fan is used for both the engineering and demonstration prototypes.

Figure 20 Heat Sink Cooling Fan

Cooling tests were performed on the three engineering prototype PV array and heat sinks using a 500 W tungsten-halogen bulb as the radiant source and the system cooling air fan at the conditions specified below:

• Radiant Source

    Single-Ended, 118 mm, Tungsten-Halogen Bulb @ 105 Volts

    Rating - 500 W @ 130 Volts

    Non-Uniform Illumination

• Heat Sink Cooling

    Cooling Air Provided by System Fan

    Inlet Air Temperature - 24 C (75 F)

    Outlet Air Temperature - 49 C (120 F)

The measured current-voltage and power-voltage curves are presented in Figure 21, 22,and 23. The results for the three arrays are compared in the Table 5. The illumination of the PV array by the tungsten-halogen bulb was non-uniform and this reduced the measured fill factor. The Voc drops at the elevated operating temperature. The third PV array performed the best and produced 16.38 W with 244 W of cooling, which is a power conversion unit efficiency of 6.7%. This efficiency is low because the tungsten-halogen produces a large fraction of its radiation at wavelengths outside the conversion band for gallium antimonide cells.

JXC PV Array # 1

Voc = 15.90 V
sc = 1.96 A
FF = 0.478
Vmax = 13.16 V
Imax = 1.13 A
Pmax = 14.91 W
Cooling = 262 W

Current (Amps)
Power (Watts)
Voltage (Volts)
Current   Power
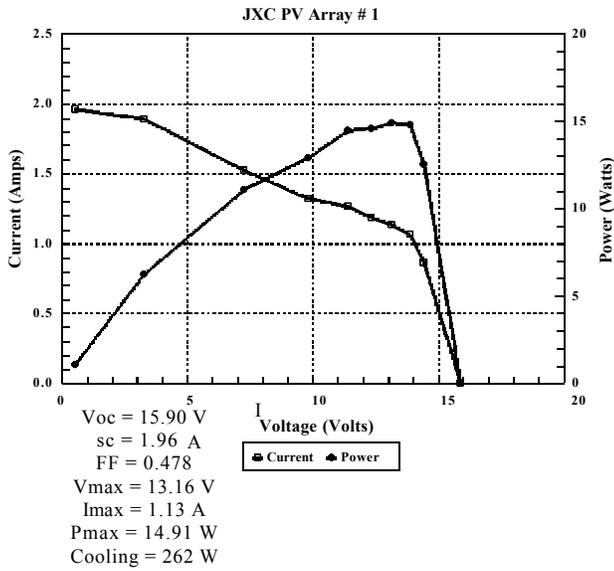
Figure 21 I-V & W-V Characteristics

JXC PV Array # 2

Voc = 15.49 V
sc = 1.95 A
FF = 0.498
Vmax = 13.09 V
Imax = 1.15 A
Pmax = 15.02 W
Cooling = 232 W

Current (Amps)
Power (Watts)
Voltage (Volts)
Current   Power
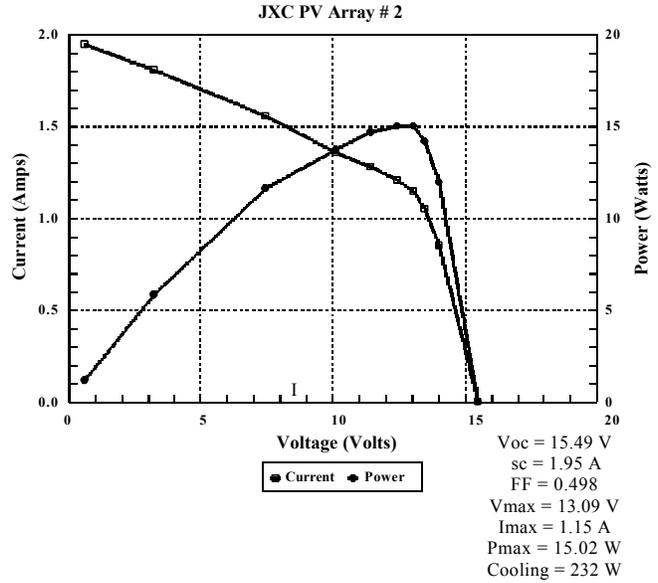
Figure 22 I-V & W-V Characteristics

JXC PV Array # 3

Current   Power

Voc = 15.58 V
Isc = 2.01 A
FF = 0.522
Vmax = 13.03 V
Imax = 1.25 A
Pmax = 16.38 W
Cooling = 244 W

Current (Amps)
Power (Watts)
Voltage (Volts)
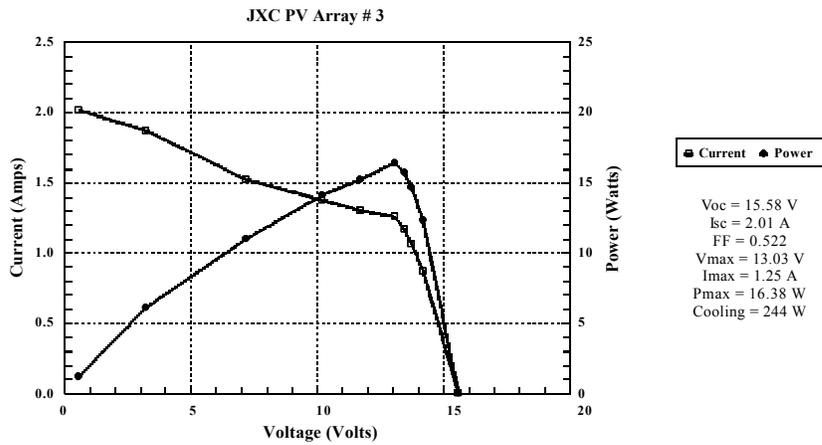
Figure 23 I-V & W-V Characteristics

Table 5 Comparison of Flash & Air-Cooled Test For PV Arrays

	PV Array #1		PV Array #2		PV Array #3	
	Flash Bulb @ 139 V	Air-Cooled Bulb @ 105 V	Flash Bulb @ 130 V	Air-Cooled Bulb @ 105 V	Flash Bulb @ 130 V	Air-Cooled Bulb @ 105 V
Voc - V	18.76	15.90	18.32	15.49	18.59	15.58
Isc – A	2.65	1.96	2.48	1.95	2.50	2.01
FF	0.523	0.478	0.502	0.498	0.457	0.522
Vmax – V	15.87	13.16	15.22	13.09	14.69	13.03
Imax – A	1.58	1.13	1.64	1.15	1.49	1.25
Pmax – W	24.99	14.91	24.98	15.02	23.15	16.38
Cooling - W	0	262	0	232	0	244

There were a number of alternative emitter options investigated for the engineering prototype. Each of these has advantages and issues associated with its use.

- Tungsten Emitter with Silicon Carbide Interior Coating
    - Selective Emitting Surface
    - High Axial Conduction Loss
- Kanthal Metal Alloy
    - Gray Body Emitting Surface
    - Low Axial Conduction
- Anti-reflective (AR) Coating on Tungsten Sputtered on Kanthal (JXC)
    - Highly Selective Emitting Surface
    - Low Axial Conduction
    - Coating Adherence Issues
- Tungsten Reradiation Emitter Around Kanthal Emitter
    - Selective Emitting Surface
    - Low Axial Conduction
    - No Coating Adherence Issues

A picture of the tungsten emitter with a silicon carbide interior coating is shown in Figure 24. A Kanthal emitter is shown in Figure 25 and a Kanthal emitter with an AR coating on sputtered tungsten, which was applied by JX Crystals is shown in Figure 25.
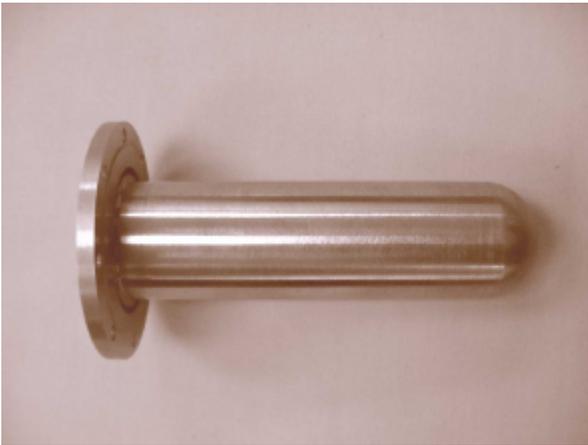
Figure 24 Tungsten Emitter with SiC Interior

Figure 25 AR-Coated Tungsten Over Kanthal Emitter

The Emitter Test Facility is pictured in Figure 26. A hot emitter on test is located in the top center of the picture. The three radiometer used for measurement are visible to the right. They provide direct measurements of the broadband radiation, silicon band radiation (< 1.1 micron wavelength) and InGaAs band (~1.0 to 1.8 micron wavelength). The temperature of the emitter is measured with the optical pyrometer visible on the right. A close-up of a Kanthal emitter in the vacuum-tight enclosure is shown unheated in Figure 27 and heated in Figure 28.
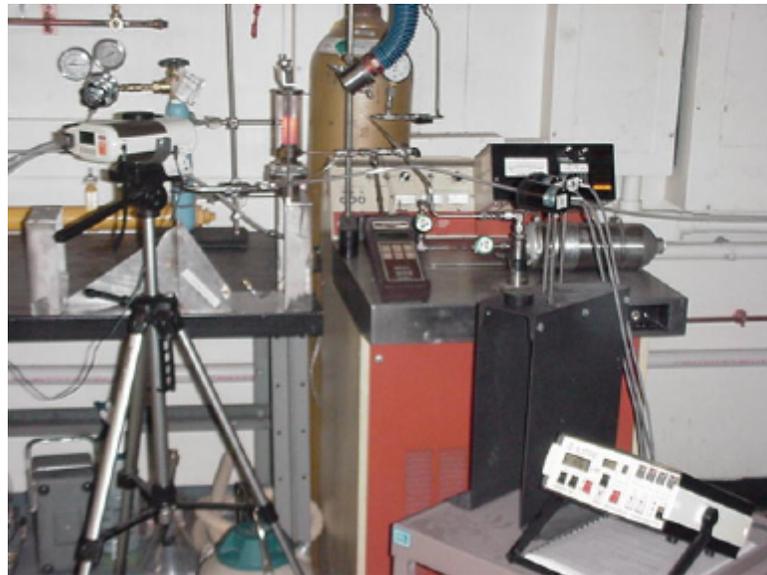
Figure 26 Emitter Test Facility

Figure 27 Emitter Test Stand

Figure 28 Kanthal Emitter Test

The temperature distribution along the emitting surface is listed in Table 6 for a Kanthal emitter and a powdered metallurgy (PM) tungsten re-radiator around a Kanthal base emitter. The temperature of both emitters are within a degree of each other at 1184 K. The temperature variation along the Kanthal is 37 K whereas the temperature variation along the PM tungsten is only 7 K. The in-band fraction of the radiation is low at 13.4% for the Kanthal and 15.9% for the PM tungsten. Table 7 shows the predicted in-band radiation per square centimeter (in-band exitance) and in-band fraction for tungsten. The data points shown on the curve for PM tungsten are in good agreement with the theoretical values. This good agreement with the theoretical values indicates that the in-band fraction will be 44% and the in-band radiation will be 4.4 W/cm^2 at the design temperature of 1700 K. Additional in-band radiation measurements are presented in Table 7 for tungsten and Kanthal.

The recuperator presented several difficult design issues. A high effectiveness is requires and the recuperator operates at high temperatures. A critical design problem is to minimize the axial heat conduction along the recuperator since this can become a sizeable heat loss in this small system. The approach taken to the recuperator design was the following:

    —   Counterflow, Single Tube with Internal and External Fins

    —   Uses Metal Alloy (Inconel) for Low Thermal Conductivity and Thin Cross-Sections

    —   Uses Interrupted Fins to Reduce Axial Conduction

Table 6 Temperature Distribution for Kanthal and Tungsten Emitters

Locations (Top to Bottom)	Kanthal Emitter Temperature (K)	Tungsten Reradiating Emitter Temperature (K)
1		1183
2	1163	1185
3	1184	1185
4	1198	1185
5	1200	1185
6	1191	1181
7	1186	1178
8	1166	1178
Average	1184	1183
Total Variation	37	7
Emitter Diameter	2.54 cm	3.05 cm
Emitter Area	38.00 cm2	45.60 cm2
In-Band Fraction	13.4%	15.9%

Table 7 Emitter In-Band Radiation Measurements

Emitter Material	Source	Temperature (K)	In-band (%)
Tungsten	Emitter	1660	44.3
Tungsten	Emitter	1680	46.0
Tungsten	Halogen Bulb	2030	57.2
Tungsten	Halogen Bulb	2110	59.8
Kanthal	Emitter	1173	13.3
Kanthal	Emitter	1180	14.7
Kanthal	Emitter	1181	14.7
Kanthal	Emitter	1188	15.5
Kanthal	Emitter	1511	17.6

The Inconel recuperator for the engineering prototype is shown in Figure 29 with the silicon carbide radiator for the burner attached.

Figure 29 Engineering Prototype Recuperator and Radiator

Designing the small propane burner for the system, which must operate with a high degree of air preheat and be quite compact, presented a number of issues. These issues and the approaches that were taken to solve them are summarized below:

- Flame Temperature
    - Achieve High Flame Temperature with High Air Preheat

- Emitter Temperature Uniformity
    - Use Internal Radiator to Balance Radiation and Convection Heat Transfer to Emitter
    - Use Thicker Cross-Section in Active Zone of Emitter with Internal Fins on Emitter

- Heat Transfer to Internal Radiator
    - Use High Swirl to Obtain Compact Combustion Zone in Radiator

- Flame Stability
    - Use Flame Holder in Low Velocity Primary Combustion Zone

- Ignition
    - Piezoelectric Spark

Initially the burner was designed without an air swirler. A simple air swirler was designed and incorporated which gave a very compact flame low in the radiator of the burner. A picture of the compact flame obtained with the air swirler is shown in Figure 30.This more compact flame resulted in more uniform emitter temperatures.

The components of the engineering prototype are shown in Figure 31. The assembled engineering prototype is shown on test in Figure 32.
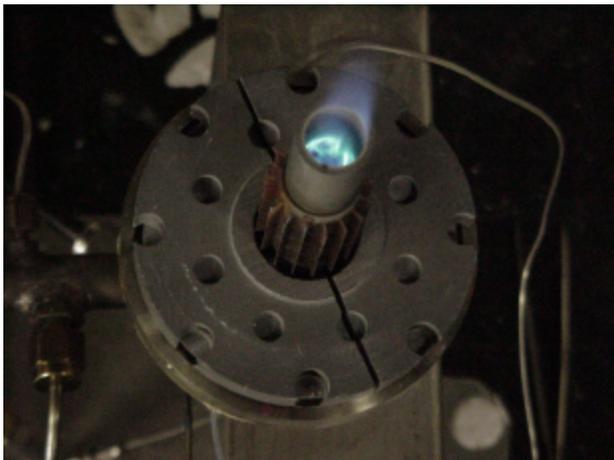
Figure 30 Flame Shape with Air Swirler

Figure 31 Engineering Prototype Components

Figure 32 Engineering Prototype Test Setup

Measurements of the heat sink pressure drop as a function of the cooling airflow rate were made with the system cooling air fan. These results are presented in Figure 33. The fan motor voltage is also shown as a function of the cooling airflow.

The assembled engineering prototype was run initially with a Kanthal emitter. The Kanthal emitter has a low in-band fraction, which results in a heat sink load that reaches the capacity of the heat sink at a relatively low emitter temperature (~1200 K). The maximum PV array power with the Kanthal emitter in the engineering prototype was ~ 5 watts. The I-V and power curves for the PV array at this operating condition are shown in Figure 34.

Ambient Temperature Test (74 F) - Pressure Probe at Center of Fins
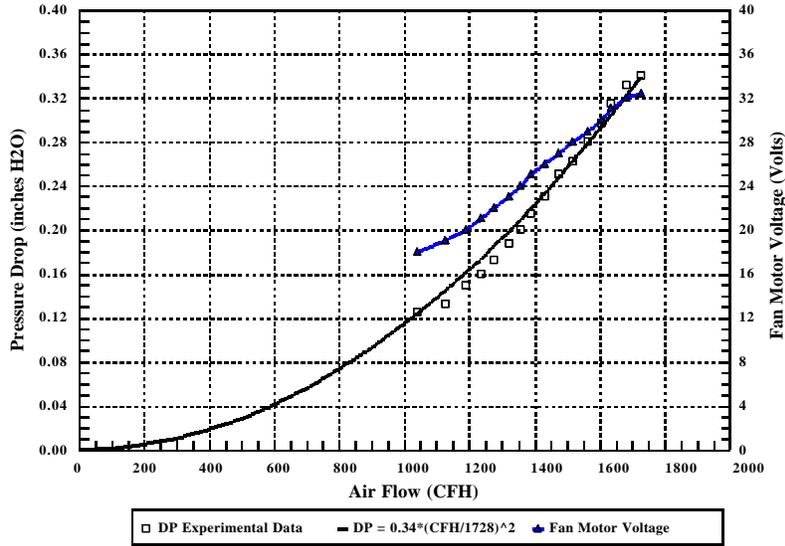
Figure 33 Heat Sink Pressure Drop vs Air Flow

Kanthal Emitter, PV Array FF = 0.449
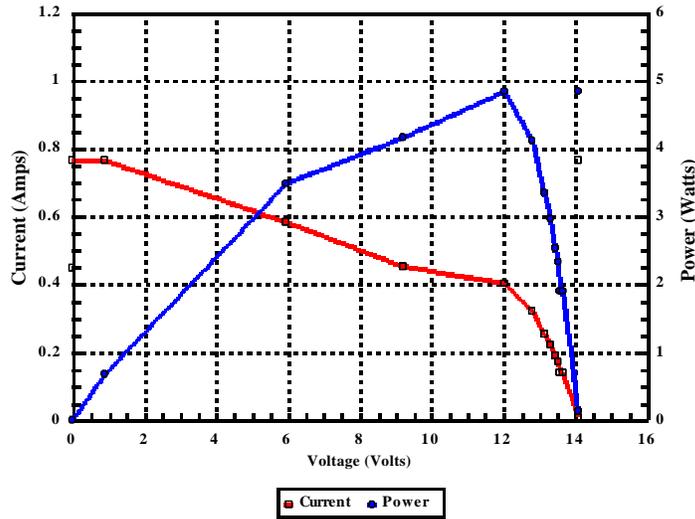
Figure 34 PV Array Current and Power vs Voltage

An AR-coated platinum foil re-radiator was made by JX Crystals for testing in the engineering prototype. It was designed to surround the Kanthal emitter with a gap at the operating temperature of ~ 0.001 inch. A picture of this re-radiator is shown in Figure 35. An uncoated platinum emitter (shown in Figure 36) was fabricated by Thermo Technologies for comparison testing. The in-band fraction with the AR coating was 15% higher than plain platinum at 1472 K. This higher emitter temperature was achieved by incorporating the air swirl improvements and using oxygen enrichment to simulate higher combustion air preheat.

Figure 35 AR Coated Platinum Re-radiator

Figure 36 Uncoated Platinum Re-radiator

With the AR-coated platinum re-radiator, combustion improvements, and oxygen enrichment, the power output from the engineering prototype was raised substantially to 14.3 watts. The fill factor on the array was also improved to 0.500 due to the more uniform emitter temperatures. The I-V and power curves for the PV array for this case are shown in Figure 37.

AR-Pt Around Kanthal Emitter, PV Array FF = 0.500
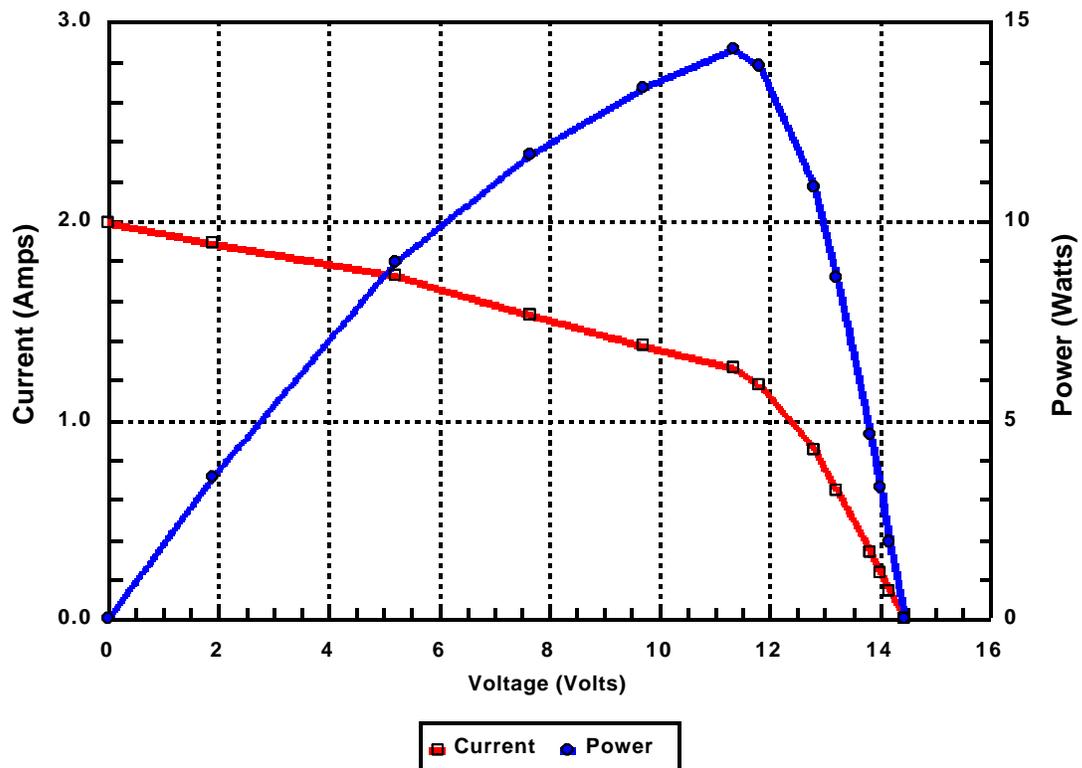
Figure 37 Engineering Prototype Test Results with AR-coated Platinum Re-radiator

6.0 DEMONSTRATION PROTOTYPE DEVELOPMENT

The demonstration prototype PV array and heat sink differs from the engineering prototype PV array and heat sink in several important ways. First it has a 44 cell flat circular end disk array in additional to a 40 cell octagonal cylinder array. Both the flat circular end disk array and octagonal cylinder array use a shingled circuit design with all cells connected in series. This approach results in a packing factor of ~ 100% compared to 75% with the flat circuit design. The net result is a 52% increase in the active array area of the full array from 42.3 cm^2 to 64.3 cm^2 with essentially the same overall dimensions for the PV array and heat sink. Second the dielectric optical filters are deposited directly on the PV cells rather than on a separate cover glasses. This provides better cooling for the filters, eliminated a transmission loss through the cover glasses, and occupies less space. Third the heat sink is made with integral copper fins rather than epoxy joined fins. This reduces the temperature gradient from the PV cells to the cooling air.

Two of the PV cell circuits for the demonstration prototype are shown in Figure 38. These show the shingled circuit design and the integral dielectric filters. The transmissivity and reflectivity of the integral filters for the demonstration prototype are shown in Figure 39. Three complete PV array and heat sinks are pictured in Figure 40.
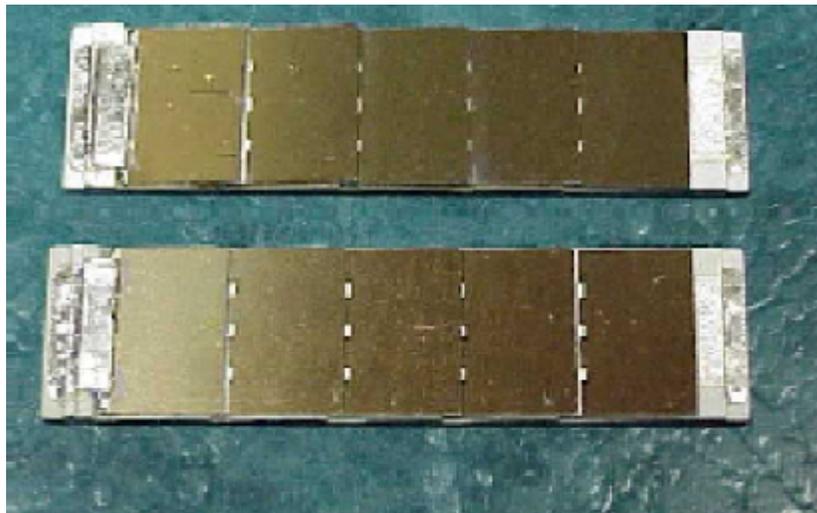
Figure 38 Demonstration Prototype PV Circuits
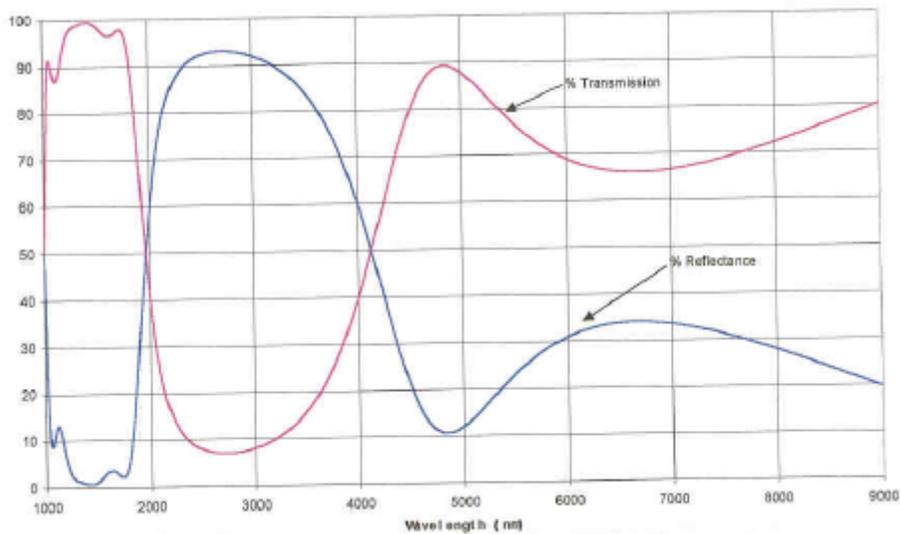
Figure 39 Transmissivity and Reflectivity of Integral Filters
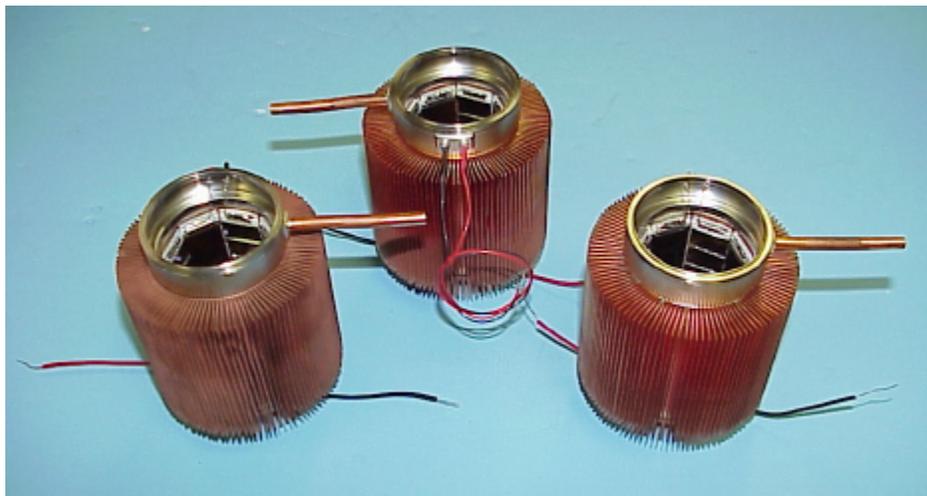
Figure 40 PV Arrays and Heat Sinks for Demonstration Prototypes

The emitter for the demonstration prototype is comprised of an AR-coated platinum foil re-radiator around a base Kanthal emitter. AR-coated platinum was chosen over AR-coated tungsten for the re-radiator, although it may have a lower in-band fraction at a given temperature. The major issues encountered with the use of tungsten were embrittlement after heating and formation of deposits of an opaque tungsten oxide layer on the optical filter surface, even though it was tested in a vacuum or an inert environment such as argon or xenon. The AR-coated platinum has the advantages that it can be used in air and remains ductile after heating.

The re-radiator for the demonstration prototype covers the top end on the Kanthal emitter as well as the side, which the re-radiator for the engineering prototype did not. JX Crystals coated platinum foils with their proprietary AR coating. Some of these foils were laser-cut to make top covers, each with three welding tabs. The other foils were rolled into cylinders and laser-welded at the overlapping seam. The top covers were then laser-welded to the cylinders at the three tab locations. A photograph of one of the completed AR-coated platinum foil re-radiators installed, over a Kanthal emitter base, is shown in Figure 41.

Figure 41 AR-Coated Platinum Foil Re-radiator for Demonstration Prototype

A Kanthal pin, which is welded to the top of the Kanthal base emitter and projects through the top of AR-coated platinum foil re-radiator, is used to secure the re-radiator in place. The pin, which is visible in the photograph, was later upset to fix the re-radiator to the Kanthal emitter base. The Kanthal base emitter is not visible in the photograph. The lower part of the Kanthal base emitter, which holds the recuperator, is covered by a low conductivity insulator and a thin-walled stainless steel cover which can be seen in the lower part of the photograph.

Characterization of PV Array and Heat Sink Performance

Prior to delivery, JX Crystals conducted flash tests on three PV array and heat sink assemblies. The results of this testing are tabulated in Table 8. The results for the top and side arrays connected in parallel are the whole array results. The results for testing the side and top (flat) arrays separately are also shown. The 44-cell top array had higher fill factors and open-circuit voltage than the 40-cell side array.

The PV array and heat sink performance was characterized using a tungsten-halogen bulb rated at 500 W at 130 volts for the radiant source. The bulb filament provides a non-uniform line source to the side cells, because the filament is shorter than the array, and a uniform point source to the top cells. The integral filters are not effective with a line or point source since they cannot reflect the out-of-band radiation back to the bulb filament. The out-of-band radiation is absorbed on the cells after multiple reflections. The cooling for the heat sink was supplied by a laboratory air supply. The air entered at $20 - 22^OC$ and the cooling airflow was varied to keep the outlet air temperature at $41 - 46^OC$.

The results of these test are summarized in Table 9 for bulb power levels from 150 to 350 watts. The total radiation and in-band radiation from the bulb were both measured. With the tungsten-halogen bulb, the fraction of the radiation detected by the silicon detector and the InGaAs detector are comparable. This is not the case for the TPV system emitter, which operates at much lower temperature than the bulb. The TPV system emitter in-band radiation is predominately in the InGaAs detector range (~1.0-1.8 microns), where the GaSb cells efficiently convert the radiant energy. For this reason the radiation detected by silicon detector was not included in the in-band for these test. For emitter tests the silicon fraction is included in the in-band fraction.

Table 8 Demonstration Prototype PV Array Performance Flash Tests at 24 C

ID	FF	Voc	Isc	Imax	Vmax	Pmax
Whole 2	.663	18.81	2.75	2.17	15.81	34.36
Cylinder 2	.631	18.37	2.08	1.51	15.92	24.12
Flat 2	.684	21.77	0.82	0.70	17.36	12.24
Whole 3	.669	19.13	3.03	2.35	16.54	38.83
Cylinder 3	.645	18.68	2.31	1.72	16.22	27.86
Flat 3	.726	21.69	0.79	0.71	17.64	12.48
Whole 4	.667	18.87	2.78	2.25	15.77	35.45
Cylinder 4	.613	18.64	2.29	1.60	16.32	26.18
Flat 4	.694	21.77	0.82	0.72	17.36	12.44

Table 9 PV Array and Heat Sink Performance Tests With Tungsten-Halogen Bulb

Bulb Power - W	150	200	250	300	350
Bulb Total Radiation – W	115	170	213	253	299
Bulb In-Band (InGaAs) Radiation – W	37.1	49.8	61.2	73.5	85.3
Bulb In-Band (InGaAs) Fraction	0.322	0.293	0.288	0.290	0.285
Total PV Array Power – W	6.7	10.2	13.1	14.9	16.0
Cooling Air Flowrate - SCFH	700	1000	1000	1000	1200
Open-Circuit Heat Sink Load – W	144	184	208	240	281
Ratio of Heat Sink Load to Total Radiation	1.25	1.09	0.98	0.95	0.94
TPV In-Band Conversion Efficiency	18.1%	20.5%	21.4%	20.3%	18.7%
TPV Conversion Efficiency Based on Total Radiation	5.8%	6.0%	6.2%	5.9%	5.3%
TPV Conversion Efficiency Based on Heat Sink Load	4.7%	5.5%	6.3%	6.2%	5.7%

The maximum PV array power measured during these tests was 16.0 watts. The maximum power level was limited by the heat sink cooling capacity because of the substantial out-of-band radiation absorbed by the array. This was due to the fact that the integral dielectric filters could not reflect the out-of-band radiation back to the small bulb element.

The TPV in-band conversion efficiency for the PV array varied from 18% to 21%. This is well below the design goal of 30%. An interesting observation is that the open-circuit heat sink load is essentially equal to the total radiation from the bulb. As a result the broadband PV array efficiency determined by either measurement is essentially the same. These are shown in the last two rows in table. The broadband PV array efficiency measurement made with the bulb was expected to be low because the integral filters cannot be effective. With an emitter, which is a much larger radiant source, the broadband PV array efficiency would be expected to be much higher when the integral filter can be effective in reflecting out-of-band radiation back to the emitter.

More detailed results for the performance of the side array and the top array are given in Tables 10 and 11 respectively. The fill factor on the side array is low because of the non-uniform source, whereas the fill factor for the top array is high. The open-circuit voltages are reduced, when compared to the flash test, because of the higher array cell temperatures. The top array operates 20°C hotter than the side array and is the limiting factor with

respect to providing adequate cooling to keep the cell below the maximum target cells temperature of 80°C. The in-band efficiency of the side array was 18% to 23% and the top array was 22% to 25%.

Table 10 Array Performance With Tungsten-Halogen Bulb

Voc – Volts	15.85	16.25	16.10	15.80	15.99
Isc – Amps	0.932	1.212	1.575	1.889	2.021
FF	0.378	0.462	0.456	0.437	0.429
Power – W	5.59	9.10	11.55	13.06	13.86
Cell Temperature – ^{O}C	52	51	58	66	64
Total Radiation to Cells – W	97	142	178	213	251
In-Band Radiation to Cells – W	31.1	41.8	51.4	61.7	71.6
TPV In-Band Conversion Efficiency	18.0%	21.8%	22.5%	21.2%	19.4%
TPV Conversion Efficiency Based on Total Radiation	5.8%	6.4%	6.5%	6.1%	5.5%

Table 11 Top Array Performance With Tungsten-Halogen Bulb

Voc – Volts	16.00	16.43	16.07	15.72	15.77
Isc – Amps	0.123	0.106	0.156	0.189	0.205
FF	0.563	0.637	0.624	0.628	0.658
Power – W	1.11	1.11	1.56	1.87	2.13
Cell Temperature – ^{O}C	75	66	78	87	88
Total Radiation to Cells – W	11.7	17.2	21.5	25.6	30.3
In-Band Radiation to Cells – W	3.75	5.04	6.19	7.44	8.64
TPV In-Band Conversion Efficiency	29.5%	22.0%	25.3%	25.1%	24.6%
TPV Conversion Efficiency Based on Total Radiation	9.5%	6.5%	7.3%	7.3%	7.0%

The burner/emitter/recuperator (BER) subassembly for the demonstration prototype was assembled to conduct additional development of the burner and to test the BER. A number of improvements were made to the burner for the demonstration prototype which resulted in increasing the temperature and temperature uniformity of the AR-coated platinum re-radiator to 1458 K $\pm$ 50 K. These included:

- Increasing the secondary air swirl to obtain more compact combustion and improved ignition
- Use of oxygen enrichment to simulate the effect of higher air preheat temperatures
- Reducing the length of the radiator to improve emitter temperature uniformity

The air swirler for the demonstration prototype is shown in Figure 42.
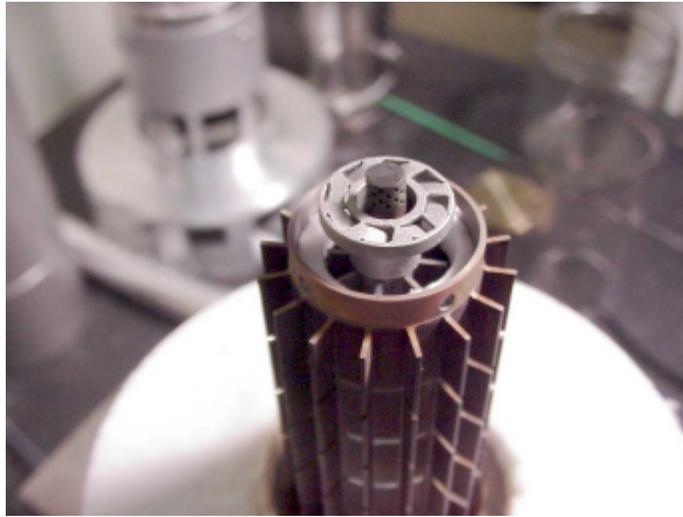
Figure 42 Final Swirler Design

Prior to installing the BER in the demonstration prototype, the BER was tested with platinum and AR-coated platinum re-radiators. A picture of one of the AR-coated platinum re-radiators being tested is shown in Figure 43. The results of the testing of the AR-coated and the uncoated platinum foil re-radiators are presented in Figure 44 at several emitter temperature levels. This figure shows the in-band radiation, total radiation, and in-band fraction of the total radiation as a function of the emitting surface temperature. The solid lines show the predicted values for uncoated platinum. The uncoated platinum data (labeled U) shows excellent agreement with the predicted curves. The AR-coated platinum data (labeled AR) shows a substantial increase in the in-band radiation and radiation fraction. The amount of the increase goes up with temperature. The improvement in the in-band radiation with the AR-coating was 57% and the improvement in the in-band fraction was 15% at 1472 K.

The BER and AR-coated platinum tests established two basic operating points with propane and air, the first without oxygen enrichment and the second with oxygen enrichment sufficient to raise the burner firing rate by 37%. These operating points were:

- Without Oxygen Enrichment
  – Maximum Firing Rate – 694 W
  – Fuel Flow – 0.0539 kg/h
  – Air Flow – 0.714 kg/h

- With Oxygen Enrichment
  – Maximum Firing Rate – 952 W
  – Fuel Flow – 0.0740 kg/h
  – Air Flow – 0.697 kg/h
  – Oxygen Flow – 0.113 kg/h

The test results at these two operating points are summarized in Table 12. The higher firing rate with oxygen enrichment raised the AR-coated platinum re-radiator (emitter) temperature to 1458 K from 1287 K. It also raised the in-band radiation fraction from 0.302 to 0.315. The BER efficiency, which is defined as the fuel heat input minus the exhaust heat content divided by the fuel heat input, was very high and over 80% for both cases. The radiative efficiency which is defined as the total (broadband) radiation divided by the fuel heat input, was much lower than expected at 33% and 48% respectively. Ideally the radiative efficiency should be close to the BER efficiency. The different between the two is mainly due to excessive axial heat conduction losses down the recuperator and the lower end of the emitter that houses the recuperator.

Figure 43 AR-Coated Platinum Emitter Test
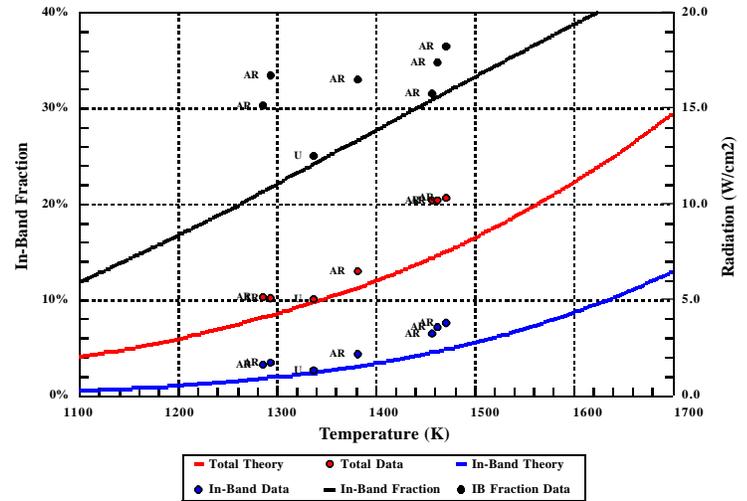
Figure 44 AR Platinum Re-radiator Tests

Table 12 Burner/Emitter/Recuperator Test Results with AR Platinum Re-radiator

Parameter	Propane/Air Combustion	Propane/Air Combustion With Oxygen Enrichment
Maximum Fuel Firing Rate – W	694	952
Exhaust Heat Content – W	131	161
AR-Pt Emitter Temperature – K	1287	1458
Total Emitter Radiation – W	228	452
In-Band Emitter Radiation – W	69	142
In-band Fraction	0.302	0.315
BER Efficiency	81.1%	83.1%
Radiative Efficiency	32.9%	47.5%

Tests with the cooling fan showed that it could deliver 1000 SCFM of airflow to the heat sink when installed in the demonstration prototype. This airflow is sufficient to provide 221 watts of cooling and keep the top array cells from overheating (~ 80°C). This is sufficient cooling to operate at the maximum firing rate without oxygen, enrichment. To operate at the oxygen enriched firing rate, a laboratory air supply had to be used to provide a higher airflow to cool the heat sink.

The BER and PV array test results were used to predict the performance of the demonstration prototype at the two firing rates. These predictions do not account for the efficiency improvements expected from of the dielectric filters on the PV cells. The results are shown in Table 13. The predicted performance is 14.5 watts from the array at a gross efficiency of 2.1% without oxygen enrichment and 27.0 watts from the array at a gross efficiency of 2.8% with oxygen enrichment.

The propane-powered venturi mixer and combustion air fan were integrated into the BER and optimized to run at the lower firing rate without oxygen enrichment. A picture of this BER in operation is shown in Figure 45. The inconel recuperator and hot silicon carbide radiator are visible through the quartz emitter substitute used for testing.

A protective quartz shield was also manufactured to protect the filters on the PV array from any possible deposits coming from the AR-platinum re-radiator. The protective quartz shield has two parts, a cylindrical piece for the side array and a flat piece for the top array. These are shown in Figure 46. No deposits were actually observed when very high purity platinum was used, although earlier test with less pure material did result in some light deposits on a shield.

Table 13 Projected Performance Based on Separate PV Array and Emitter Test Results

Parameter	Propane/Air Combustion	Propane/Air Combustion With Oxygen Enrichment
Maximum Fuel Firing Rate – W	694	952
Radiative Efficiency	32.9%	47.5%
Total Emitter Radiation – W	228	452
In-Band Fraction **Without Benefit of Dielectric Filters**	0.302	0.315
In-Band Radiation – W	69	142
In-Band PV Array Efficiency	21%	19%
Projected PV Array Power – W	14.5	27.0
Projected Gross TPV System Efficiency **Without Benefit of Dielectric Filters**	2.1%	2.8%
Heat Sink Load to Total Radiation Ratio	0.97	0.94
Projected Heat Sink Load – W **Without Benefit of Dielectric Filters**	221	425

Figure 45 Propane-Powered Venturi Mixer and Combustion Air Fan Integration
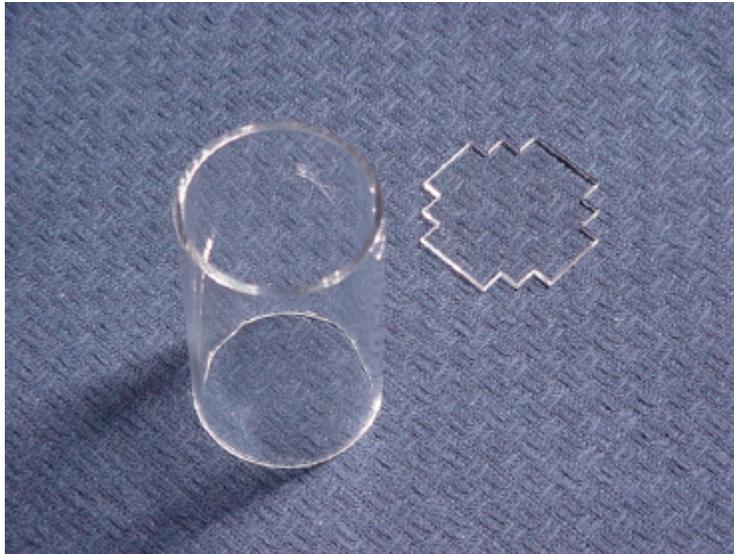
Figure 46 Protective Quartz Sheild

All the parts that make up the demonstration prototype are shown in Figure 47 arranged in an exploded view. The completed assembled prototype is shown in Figure 48. It is shown mounted on a stand that holds it in a stable vertical position. The demonstration prototype is designed to run in any orientation.

The demonstration prototype weighs 2.65 kg as built. It has been estimated that this weight could be reduced to 1.36 kg by using aluminum instead of copper for the heat sink and instead of stainless steel for housings and other parts.

Figure 47 Demonstration Prototype Components

Figure 48 Assembled Demonstration Prototype

The demonstration prototype was tested at the two firing rates (694 W and 952 W). At both firing rates, the demonstration prototype was run with and without the top array being active. The top array was made inactive by inserting a piece of thermal insulation between it and the emitter. The results of these tests are summarized in Table 14. At the lower firing rate the system produced a maximum power of 13 watts at a gross efficiency of 1.9% with the top array active. At the lower firing rate the system produced a maximum power of 28 watts with the top array inactive. Inactivating the top array at the higher firing rate apparently allowed the emitter to run at a sufficiently

higher temperature to produce more power with just the side array. It was not possible to actually measure this temperature and the one shown is from the separate emitter tests.

The I-V and power versus voltage curves for the higher firing rate are shown on Figure 49. The peak power of 48 watts occurs at 12 volts. The fill factor was 0.548 indicating that further improvements could be made if the emitting surface temperature could be made more uniform.

Table 14 Summary of Demonstration Prototype Laboratory Test Results

Parameter	Propane/Air Combustion		Propane/Air Combustion With Oxygen Enrichment	
Top PV Array		Blocked		Blocked
Voc – Volts	15.74		15.70	
Isc – Amps	0.156		0.222	
FF	0.585		0.568	
Power –W	1.44		1.98	
Cell Temperature – C	83		90	
Side PV Array				
Voc – Volts	15.85	16.30	16.00	15.72
Isc – Amps	1.130	1.361	1.823	3.259
FF	0.645	0.542	0.641	0.549
Power –W	11.55	12.02	18.71	28.11
Cell Temperature – C	56	52	62	77
Total Array Power – W	12.99	12.02	20.69	28.11
Emitter (Separate Test)				
Temperature – K	1287	1287	1458	1458
Broadband Radiation – W	228.2	202.2	452.2	400.8
In-band Radiation – W	69.0	61.1	142.4	126.2
In-Band Fraction	30.2%	30.2%	31.5%	31.5%
Fuel Heat Input – W	694	694	952	952
Heat Sink Load – W	221	196	425	377
Exhaust Heat Content – W	131	141	161	201
BER Efficiency	81.1%	79.7%	83.1%	78.9%
Radiative Efficiency	32.9%	29.1%	47.5%	42.1%
In-Band Array Efficiency	18.8%	19.7%	14.5%	22.3%
Broadband Array Efficiency	5.7%	5.9%	4.6%	7.0%
Gross Efficiency	1.9%	1.7%	2.2%	3.0%

AR-Pt Reradiator, Argon, Insulated Top, Side PV Array FF = 0.548
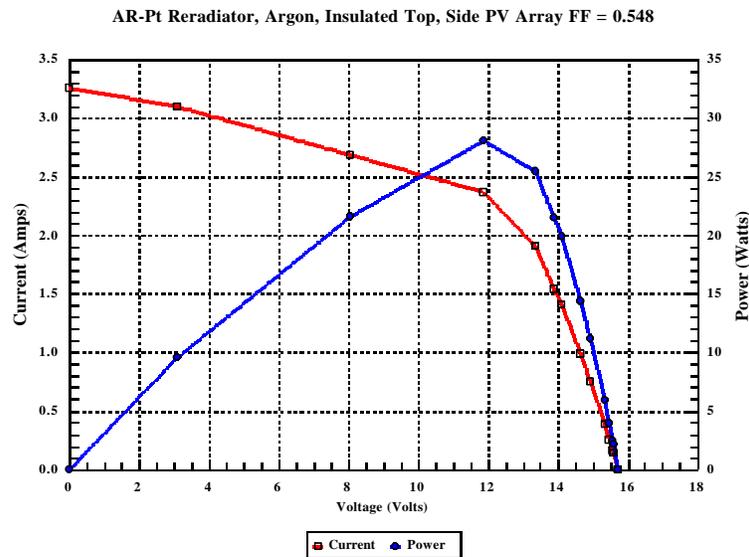
Figure 49 Demonstration Prototype - Side PV Array Characteristics with Oxygen Enriched Combustion

7.0 CONCLUSION AND RECOMMENDATIONS

The performance of the demonstration prototype at the two firing rates is compared to the design goals in Table 15. These result show that significant improvements still can be made in the radiative efficiency by reducing heat losses and in the in-band radiation fraction at the array, after the filters, by using a much higher efficiency dielectric filter with more layers. A comparison of the system test results to the projections made from the component test is given in Table 16. The fact that the gross efficiency of the system is only slightly higher than that projected from the component tests, indicated that the dielectric filter are not very effective with the AR-coated platinum emitter.

Table 15 TPV System Efficiency Status

Efficiency Parameter	Design Goals	Demo Prototype with Propane/Air	Demo Prototype with Oxygen Enrichment
Radiative Efficiency	60%	32.9%	42.1%
Broadband Array Efficiency	15%	5.7%	7.0%
Gross Efficiency	9.0%	1.9%	3.0%
BER Efficiency	68%	81.1%	78.9%
In-Band Fraction @ Emitter		30.2%	31.5%
In-Band Fraction @ Array	50%		
In-Band Array Efficiency	30%	18.8%	22.3%
Parasitic Power/Gross Power	20%		
Net Efficiency	7.2%		

Table 16 Comparison of Projections from Component Performance Tests to Prototype Test Results

Parameter	Propane/Air Combustion		Propane/Air Combustion With Oxygen Enrichment	
	Projections from Component Tests	TPV Demo System Test Results	Projections from Component Tests	TPV Demo System Test Results
Top PV Array Blocked	No	No	No	Yes
Maximum Fuel Firing Rate – W	694	694	952	952
PV Array Power – W	14.5	13.0	27.0	28.11
Gross TPV System Efficiency	2.1%	1.9%	2.8%	3.0%

The conclusions and recommendation based on the test results are:

- BER Axial Thermal-Conduction Heat Losses Must be Reduced to Increase Radiative Efficiency
    - Segment Recuperator and Lower Section of Emitter
    - Improved Insulation
- Spectral Control Must be Improved to Increase PV Array In-Band and Broadband Efficiencies
    - Improved Dielectric Filters by Using More Layers
    - Add End Reflectors
    - Reduce Emitter Diameter to Operate at Higher Temperature and Correspondingly Higher In-Band Fraction
    - Long Term: AR-Coated Tungsten in Hermetic Chamber
- Achieve Higher and More Uniform Emitter Temperature for Better Fill Factors and PV Array In-Band and Broadband Efficiencies
    - Improve Recuperator Effectiveness Obtain Higher Air Preheat
    - Improve Combustion Intensity for Better Temperature Uniformity

The gross efficiency and PV array power, measured with the AR-platinum emitting surface at the higher firing rate, are compared to the values projected at higher emitting surface temperatures in Figures 50 and 51 respectively. At the design temperature level of 1700 K, the gross efficiency would be ~7%. The gross power, however, would be much higher than needed. This strongly indicates that a smaller diameter emitter, which would run hotter at the same firing rate, would produce the required power at a higher efficiency.
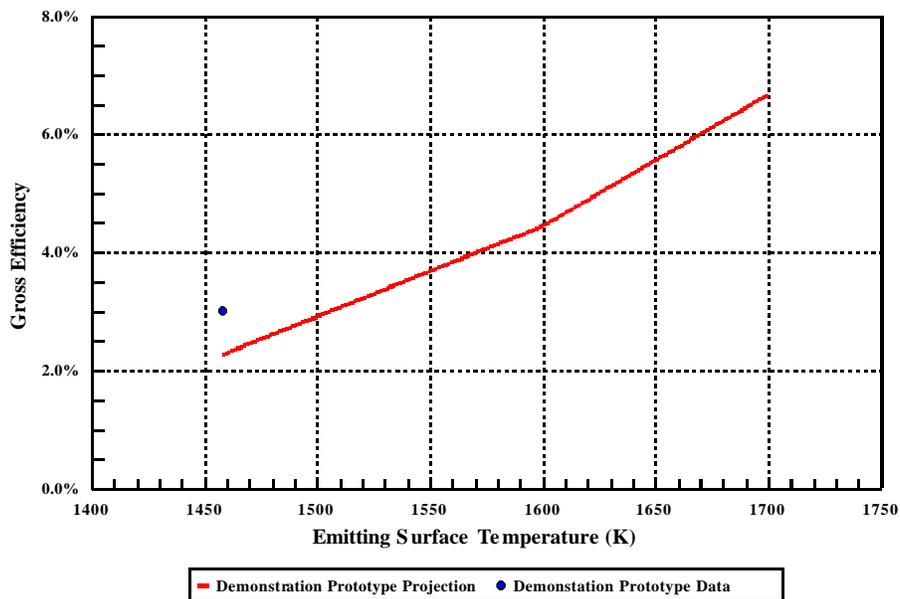
Figure 50 TPV System Efficiency for AR-Platinum Emitting Surface
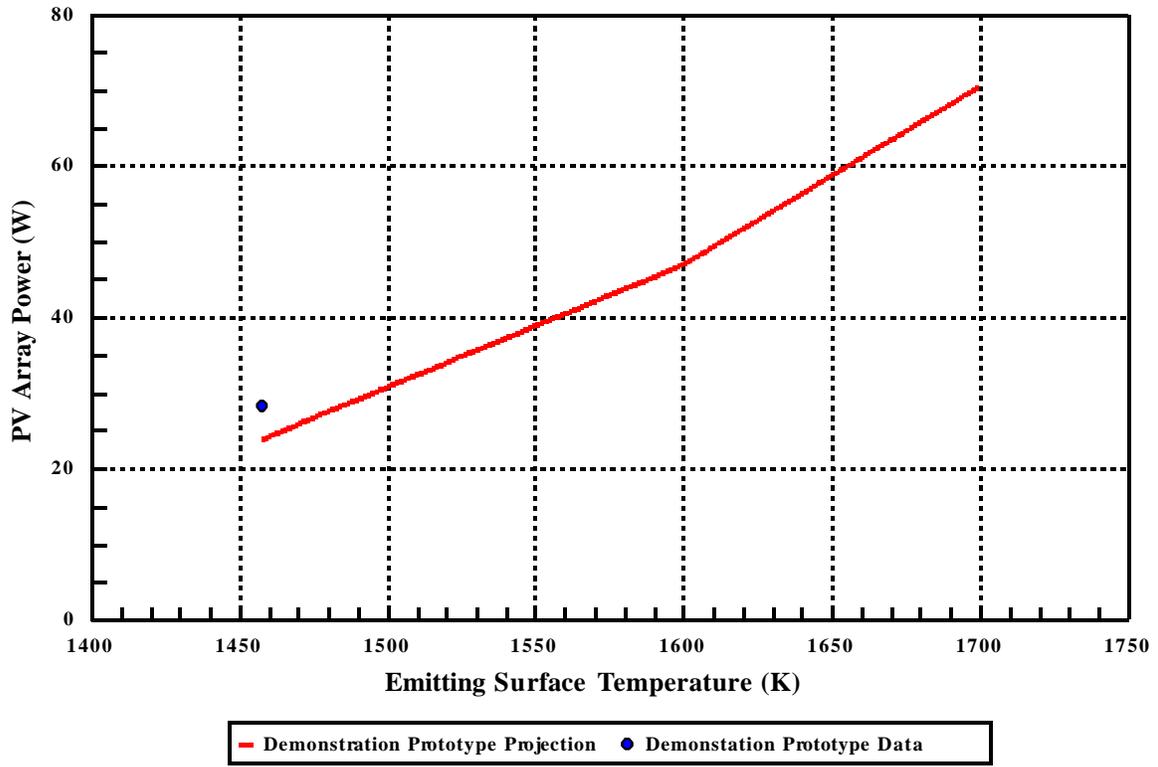
Figure 51 PV Array Power for AR-Platinum Emitting Surface

REPORT DOCUMENTATION PAGE

Public reporting burden for this collection of information is estimated to average 1 hour per response, including the time for reviewing instructions, searching existing data sources, gathering and maintaining the data needed, and completing and reviewing the collection of information. Send comments regarding this burden estimate or any other aspect of this collection of information, including suggestions for reducing this burden, to Washington Headquarters Services, Directorate for Information Operations and Reports, 1215 Jefferson Davis Highway, Suite 1204, Arlington, VA 22202-4302, and to the Office of Management and Budget, Paperwork Reduction Project (0704-0188), Washington, DC 20503.

1. AGENCY USE ONLY (Leave blank)	2. REPORT DATE	3. REPORT TYPE AND DATES COVERED
	August 2001	Final Contractor Report

4. TITLE AND SUBTITLE

Development and Demonstration of a 25 Watt Thermophotovoltaic
Power Source for a Hybrid Power System

5. FUNDING NUMBERS

WU–755–1A–02–00
NAS3–97197

6. AUTHOR(S)

Edward Doyle, Kailash Shukla, and Christopher Metcalfe

7. PERFORMING ORGANIZATION NAME(S) AND ADDRESS(ES)

Thermo Power Corporation
Thermo Technologies Division
45 First Avenue
Waltham, Massachusetts 02454–9046

8. PERFORMING ORGANIZATION REPORT NUMBER

E–12910

9. SPONSORING/MONITORING AGENCY NAME(S) AND ADDRESS(ES)

National Aeronautics and Space Administration
Washington, DC 20546–0001

10. SPONSORING/MONITORING AGENCY REPORT NUMBER

NASA CR—2001-211071
TR04–2001

11. SUPPLEMENTARY NOTES

Project Manager, David Wilt, Power and On-Board Propulsion Technology Division, NASA Glenn Research Center, organization code 5410, 216–433–6293.

12a. DISTRIBUTION/AVAILABILITY STATEMENT

Unclassified - Unlimited
Subject Category: 44   Distribution: Nonstandard

Available electronically at http://gltrs.grc.nasa.gov/GLTRS

This publication is available from the NASA Center for AeroSpace Information, 301–621–0390.

12b. DISTRIBUTION CODE

13. ABSTRACT (Maximum 200 words)

The development of a propane-fueled, 25 W thermophotovoltaic (TPV) power source for use in a hybrid power system is described. The TPV power source uses a platinum emitting surface with an anti-reflective coating to radiate to gallium antimonide photocells, which converts the radiation to electric power. The development program started with the design and fabrication of an engineering prototype system. This was used as a component development vehicle to develop the technologies for the various components. A 25 W demonstration prototype was then designed and fabricated using the most advanced component approaches. The designs and test results from this development program are discussed.

14. SUBJECT TERMS

Thermophotovoltaics; TPV; Power sources

15. NUMBER OF PAGES

51

16. PRICE CODE

17. SECURITY CLASSIFICATION OF REPORT	18. SECURITY CLASSIFICATION OF THIS PAGE	19. SECURITY CLASSIFICATION OF ABSTRACT	20. LIMITATION OF ABSTRACT
Unclassified	Unclassified	Unclassified	

NSN 7540-01-280-5500

Standard Form 298 (Rev. 2-89)
Prescribed by ANSI Std. Z39-18
298-102